# Stable isotope and calcareous nannofossil assemblage record of the late Paleocene and early Eocene (Cicogna section)

Claudia Agnini[12*], David J. A. Spofforth[3], Gerald R. Dickens[4,5], Domenico Rio[1], Heiko Pälike[6], Jan Backman[5], Giovanni Muttoni[7,8], Edoardo Dallanave[9]

[1] Dipartimento di Geoscienze, Università di Padova, Padova, Italy.

[2] Istituto di Geoscienze e Georisorse- Padova, CNR, Padova, Italy

[3] Robertson - CGG GeoSpec, Llandudno, United Kingdom

[4] Department of Earth Sciences, Rice University, Houston, Texas, USA.

[5] Department of Geological Sciences, Stockholm University, Stockholm, Sweden

[6] MARUM, University of Bremen, Bremen, Germany

[7] Dipartimento di Scienze della Terra "Ardito Desio", Università Statale di Milano, Milano, Italy

[8] ALP – Alpine Laboratory of Paleomagnetism, Peveragno (CN), Italy

[9] Ludwig-Maximilians, Universität München, München, Germany

[*]Corresponding author: C. Agnini, Dipartimento di Geoscienze, Università di Padova, 35131 Italy. (claudia.agnini@unipd.it)

**Abstract.** We present records of stable carbon and oxygen isotopes, $CaCO_3$ content, and changes in calcareous nannofossil assemblages across an 81 m thick section of upper Paleocene-lower Eocene marine sedimentary rocks now exposed along the Cicogna Stream in northeast Italy. The studied stratigraphic section represents sediment accumulation in a bathyal hemipelagic setting from approximately 57.5 to 52.2 Ma, a multi-million-year time interval characterized by perturbations in the global carbon cycle and changes in calcareous nannofossil assemblages. The bulk carbonate $\delta^{13}C$ profile for the Cicogna section, once placed on a common time scale, resembles that at several other locations across the world, and includes both a long-term drop in $\delta^{13}C$, and multiple short-term carbon isotope excursions (CIEs). This precise correlation of widely separated $\delta^{13}C$ records in marine sequences results from temporal changes in the carbon composition of the exogenic carbon cycle. However, diagenesis has likely modified the $\delta^{13}C$ record at Cicogna, an interpretation supported by variations in bulk carbonate $\delta^{18}O$, which do not conform to expectations for a primary signal. The record of $CaCO_3$ content reflects a combination of carbonate dilution and dissolution, as also inferred at other sites. Our detailed documentation and statistical analysis of calcareous nannofossil assemblages show major differences before, during and after the Paleocene Eocene Thermal Maximum. Other CIEs in our lower Paleogene section do not exhibit such a distinctive change; instead, these events are sometimes characterized by variations restricted to a limited number of taxa and transient shifts in the relative abundance of primary assemblage components. Both long-lasting and short-lived modifications to calcareous nannofossil assemblages preferentially affected nannoliths or holococcoliths such as *Discoaster, Fasciculithus, Rhomboaster/Tribrachiatus, Spenolithus* and *Zygrhablithus*, which underwent distinct variations in abundance as well as permanent evolutionary changes in terms of appearances and disappearances. By contrast, placoliths such as *Coccolithus* and *Toweius*, which represent the main component of the assemblages, were characterized by a gradual decline in abundance over time. Comparisons of

detailed nannofossil assemblage records at the Cicogna section and at ODP Site 1262 support the idea that variations in the relative and absolute abundances, even some minor changes, were globally synchronous. An obvious link is through climate forcing and carbon cycling, although the linkages between variations in calcareous nannoplankton, changes in $\delta^{13}C$ records and oceanography will need additional work.

**INDEX TERMS**

Paleocene, Eocene, calcareous nannofossils, stable isotopes, paleoclimate, Tethys

## 1 INTRODUCTION

A remarkable interval of global warming occurred from the middle Paleocene to the early Eocene, between approximately 59 and 51 million years ago (Ma). This inference comes from a variety of proxies (Huber and Caballero, 2011; Hollis et al., 2012), including the stable oxygen isotope ($\delta^{18}O$) composition of benthic foraminifera (**Figure 1**). The precise timing of the long-term temperature rise remains somewhat unconstrained, because absolute ages across the early Eocene remain unsolidified. Throughout this work, we assume that the Option-1 (WO-1) time scale presented by Westerhold et al. (2008) is correct (**Table 1**), but acknowledge that an offset of ca 400 kyr may occur within the time interval of interest (Vandenberghe et al., 2012). Debate also surrounds the magnitude and distribution of the temperature warming. Earth's surface temperatures, at least at high latitudes and in the deep sea, seem to have risen by at least 6°C from ca. 59 to 51 Ma (Zachos et al., 2008; Bijl et al., 2009; Huber and Caballero, 2011; Hollis et al., 2012). Indeed, the latter date marks the acme of the Early Eocene Climatic Optimum (EECO), the warmest sustained time interval of the Cenozoic (Zachos et al., 2008; Cramer et al., 2009; Hollis et al., 2012). Such a rise in

69 temperature is not obvious at low latitudes with current data (Pearson et al., 2007; Huber et al.,
70 2011).

71 Somehow related to long-term global warming were a series of major perturbations in the
72 global carbon cycle, as clearly indicated by stable carbon isotope ($\delta^{13}C$) records in benthic
73 foraminifera (**Figure 1**) and bulk carbonate in numerous marine sediment sequences (Shackleton,
74 1986; Corfield, 1994; Cramer et al., 2003; Zachos et al., 2008; 2010; Westerhold et al., 2011; Slotnick
75 et al., 2012). An overall increase in $\delta^{13}C$ occurred through most of the Paleocene, which climaxed in
76 a Cenozoic high at ca. 57.5 Ma (Westerhold et al., 2011), commonly referred to as the Paleocene
77 carbon isotope maximum (PCIM). From this time, $\delta^{13}C$ generally decreased to ca. 52.5 Ma. However,
78 when examined at higher temporal resolution, multiple $\delta^{13}C$ records show several short-term (<200
79 kyr) negative carbon isotope excursions (CIEs) (Cramer et al., 2003; Lourens et al., 2005; Nicolo et
80 al., 2007; Agnini et al., 2009; Zachos et al., 2010; Slotnick et al., 2012). Some of these CIEs clearly
81 coincided with rapid warming (above references). The most prominent and most widely
82 documented example of these "hyperthermals" was the Paleocene-Eocene Thermal Maximum
83 (PETM) at ca. 55.5 Ma, but other apparently similar events occurred at ca. 53.7 Ma (H1 or Eocene
84 Thermal Maximum 2, ETM-2), and at ca. 52.5 Ma (K/X, sometimes called ETM-3).

85 The early Paleogene in general, and the hyperthermals in particular, have attracted
86 considerable geoscience research. On one level, this is because these time intervals represent a
87 range of possible past analogues for understanding the effects of global warming and massive
88 carbon emissions (cf. Keeling and Whorf, 2004; Zachos et al., 2008). On another level, this is because
89 the long-term and short-term temperature and carbon cycle perturbations provide new
90 perspectives for how systems on Earth's surface operate. The PCIM probably represents a
91 tremendous storage of $^{13}C$-depleted carbon somewhere on Earth's shallow surface (Shackleton,
92 1986; Kurtz et al., 2003; Komar et al., 2013). In turn, the CIEs probably signify rapid and large inputs

of $^{13}$C-depleted carbon into the ocean and atmosphere (Dickens et al., 1997; Lourens et al., 2005; Zeebe et al., 2009). The middle Paleocene through early Eocene shows us that Earth's climate and carbon reservoirs were extremely dynamic during past times of global warmth. However, the composition and whereabouts of large quantities of transferable $^{13}$C-depleted carbon (e.g., seafloor methane, peat, permafrost) remain uncertain (above references). Indeed, it is not clear if and how the long-term and short-term carbon cycle perturbations were related to one another, or to Earth surface temperatures.

The above context presents a series of basic questions to the geoscience community. Two of these are the focus of our study: (1) What is the correct template for understanding carbon cycling during the early Paleogene? Major changes in fluxes of $^{13}$C-depleted carbon to the ocean or atmosphere should give predictable and coherent signals in the $\delta^{13}$C of carbon-bearing phases across Earth, as well as the distribution of carbonate dissolution on the seafloor. This is not yet established. For example, several recently published $\delta^{13}$C records (Kirtland-Turner et al., 2014; Slotnick et al., 2015a; Payros et al., 2015) do not precisely correlate with those at other locations (Cramer et al., 2003; Zachos et al., 2010; Slotnick et al., 2012, 2015b), at least with available stratigraphy. (2) How did marine calcifying organisms respond to major early Paleogene perturbations in temperature and carbon cycling, both in terms of evolution and preservation? The prominent changes in temperature and carbon fluxes almost assuredly caused large variations in seawater pH and carbonate ion concentration ($CO_3^{2-}$) (Dickens et al., 1997; Zachos et al., 2005; Kump et al., 2009; Zeebe et al., 2009; Leon-Rodriguez and Dickens, 2010; ; Hönisch et al., 2012; Pälike et al., 2012), although the response should depend on location and carbon fluxes involved (Dickens, 2000; Zeebe and Westbroek, 2003; Komar et al., 2013). Such changes might also affect the ability of living organisms to calcify (Riebesell et al., 2000, 2008; Kleypas et al., 2006; Iglesias-Rodriguez et al.,

2008; Stillman and Paganini, 2015), which might impact the fossil record (Agnini et al., 2006; Raffi and De Bernardi, 2008; Erba et al., 2010; Hönisch et al., 2012).

In regards to both questions, calcareous nannoplankton are an obvious group of organisms to focus on. This is because they are a main component of open ocean primary production (Milliman, 1993; Winter et al., 1994; Rost and Riebesell, 2004), because they are the dominate the output of carbonate in the ocean (Ziveri et al., 1999; Hay, 2004), and because they exhibit marked changes in species composition from the middle Paleocene through the early Eocene (Romein, 1979; Aubry, 1998, Bown et al., 2004; Gibbs et al., 2012). While numerous studies have examined calcareous nannofossils across the PETM from different perspectives (e.g., Bralower, 2002; Stoll and Bains, 2003; Gibbs et al., 2006a; 2006b; Agnini et al., 2007a; Mutterlose et al. 2007; Bown and Pearson, 2009; Jiang and Wise, 2009, Self-Trail et al., 2012), the relationship between these organisms and carbon cycle perturbations before and after this short-lived warming episode remain poorly documented (Gibbs et al., 2012). It seems possible that the high rate of calcareous nannofossil taxonomic evolution (appearances and extinctions), as well as distinct changes in calcareous nannofossil abundance patterns may provide excellent stratigraphic control across the early Paleogene (Bukry, 1973; Perch-Nielsen, 1985; Backman, 1986, Agnini et al., 2014). Moreover, if the exact relationship between changes in nannofossil assemblages and global carbon cycle perturbations were known, key time intervals could be rapidly identified for more detailed work. Finally, changes in calcareous nannofossils across the early Paleogene provide insights about the response of an important part of the sediment forming marine biota to changes in climate and carbon cycling.

Very few stratigraphic sections presently have detailed and coupled records of stable isotopes, carbonate content, and calcareous nannofossil abundances across the broad late Paleocene-early Eocene interval. The two notable exeptions are Ocean Drilling Program (ODP) Site 1262 (southeast

Atlantic) (Agnini et al., 2007b; Zachos et al., 2010) and Deep Sea Drilling Project (DSDP) Site 577 (northwest Pacific) (Shackleton, 1986; Dickens and Backman, 2013) (**Figure 2**). Here we present geochemical records ($\delta^{13}C$, $\delta^{18}O$ and $CaCO_3$ content) and calcareous nannofossil census data from the Cicogna section in northeast Italy (**Figures 2, 3**). These data are compared with similar information from Sites 1262 and 577. We show that the Cicogna section provides an important template for understanding potential relationships between climate, carbon cycling and the biotic evolution of calcareous nannoplankton.

## 2 THE CICOGNA SECTION

The Cicogna section crops out along the Cicogna Stream near the village of Tassei in the Belluno Province, northeast Italy (**Figure 3**). From a regional geological perspective, the sedimentary rocks of this section belong to the Belluno Basin. This basin represents part of a paleogeographic domain that formed when Jurassic rifting created a series of N–S oriented structural highs (platforms) and lows (basins), which persisted through much of the Paleogene (Bernoulli and Jenkyns, 1974; Bernoulli et al., 1979; Winterer and Bosellini, 1981). Importantly, from the Cretaceous to the middle-late Eocene, expanded deep sea sediment successions accumulated within the basins at nominally 30°N latitude (Stefani and Grandesso, 1991; Agnini et al., 2006; 2011; Zattin et al., 2006).

The Cicogna section consists of two lithostratigraphic units **(Figure 3**). The lower portion is a well-exposed upper Paleocene and lower Eocene unit referred to as Scaglia Rossa *sensu lato* (**Figures 3, 4**) (Giusberti et al., 2007; Dallanave et al., 2009). Based on benthic foraminiferal assemblages, the early Paleogene marls of this unit represent lithified pelagic and hemipelagic sediment that accumulated at middle to lower bathyal water depth, likely between 600 m and 1000 m and not deeper than 1500 m (Giusberti et al., 2007; 2015). The upper portion is a thick early to middle

164 Eocene unit called the Belluno Flysch (**Figures 3, 4**). This unit represents a synorogenic deposit on
165 the flanks of the former Trento and Friuli platforms (Grandesso, 1976; Doglioni and Bosellini, 1987).
166 Once corrected for bed strike and dip (ca. 315°N; ca. 45°) and bends in the stream, the Scaglia
167 Rossa at Cicogna measures 80 m in terms of stratigraphic height (Dallanave et al., 2009). The Belluno
168 Flysch measures 1 m in the Cicogna section. Furthermore, the section of interest can be subdivided
169 into several subunits (**Figure 4**). The lower 20 m is comprised of distinctive alternating beds of gray-
170 greenish to purple marls and calcareous marls, the latter defined by carbonate contents higher than
171 60% (**Figure 3c**). This is overlain by approximately 9 m of pink-red marls with much less lithologic
172 alternation. At 28.7 m, the sedimentary package is broken sharply by an approximately 3 m thick
173 red to brownish-red interval of clayey marls with sporadic grey-green cm-scale spots and lenses
174 (**Figure 3f, g**). This has been called the Clay Marl Unit (CMU), and records the core of the prominent
175 negative $\delta^{13}C$ excursion associated with the PETM at multiple outcrop sites within the Belluno Basin
176 (Agnini et al., 2006; 2007a; Giusberti et al., 2007). Above the CMU, from 31.7 to 39.2 m, the section
177 continues with deposition of rhythmic alternations of marls and calcareous marls (**Figure 3g**). Above
178 this 8.5 m thick interval, at ca. 40.5 m, spatic calcite crystals occur. Generally, couplets of marl and
179 calcareous marl couplets become less evident from 40.5 m until 54 m, where such couplets reoccur
180 (**Figure 3d**). At 75.5 m, a thin calcarenitic bed is encountered, presaging the onset of the Belluno
181 Flysch. This turbidite is followed by a temporary return to hemipelagic sedimentation that ends at
182 80.6 m. Above, sedimentation of the Belluno Flysch begins in earnest (**Figures 3b, 4**).
183 The basic stratigraphy of the Scaglia Rossa in the Cicogna section, including both polarity chron
184 boundaries and key calcareous nannofossil biohorizons has been published (Giusberti et al., 2007;
185 Dallanave et al., 2009). The combined biomagnetostratigraphy indicates that the 81 m of interest
186 spans polarity Chron C25r to Chron 23r, and calcareous nannofossil biozones CP6 to CP10 (Okada
187 and Bukry, 1980) or CNP10 to CNE4 (Agnini et al., 2014). Thus, the section represents a 5.3 million

188 year (Myr) long time interval, from about 57.5 to 52.2 Ma on the W0-1 time scale. This also implies
189 an average sedimentation rate (SR) of ca. 15 m/myr. Although the deposition of hemipelagic
190 sediment might suggest relatively constant SRs over time, the PETM and possibly other
191 hyperthermal events in the Belluno Basin were characterized by higher SRs (Giusberti et al. 2007;
192 Agnini et al., 2009; Tipple et al., 2011; Krishnan et al., 2015).

193 The Scaglia Rossa at Cicogna appears to record fairly continuous sediment accumulation at
194 moderately high deposition rates. This is important because it affords longer time duration than
195 most shallow ocean sites, greater time resolution than most deep ocean sites (**Figure 2**), and an
196 overall different environmental setting. Many early Paleogene records, especially those from paleo-
197 shelf environments, such as in Egypt (e.g, Aubry and Salem, 2012) and New Jersey (Mixon and
198 Powars, 1994; Harris et al., 2010), or from early deep sea drilling expeditions, such as in the Indian
199 Ocean (Slotnick et al., 2015b), are discontinuous, either because of hiatuses or core gaps. Much of
200 the detailed work and current understanding of stable carbon isotope stratigraphy and calcareous
201 nannofossil variations across the broad early Paleogene, therefore, has come from deep-sea drilling
202 sites with multiple holes but slow sedimentation rates, although we note the work in Clarence
203 Valley, New Zealand (**Figure 2**), another area that contains several paleo-slope sections with
204 moderately high sedimentation rates (Nicolo et al., 2007; Slotnick et al., 2012, 2015b; Dallanave et
205 al., 2015). For the Cicogna section, detailed stable isotope and $CaCO_3$ records are currently lacking,
206 as well as detailed calcareous nannofossil assemblage information, which we present here.
207
208 ## 3 MATERIAL AND METHODS
209
210 ### 3.1 Samples
211

A total of 492 samples were chiseled from outcrops along the section. Samples were selected so as to be as fresh and unaltered as possible. This included chipping off weathered surfaces while in the field. Each sample was calibrated to height (**Figure 4**). Samples then were split, with one portion powdered in an agate ball mill, and subsequently freeze-dried.

### 3.2 Geochemistry

Each powdered samples was analyzed for bulk sediment stable isotope composition at the Stable Isotope Laboratory, University of Southampton, UK. A known mass (~80 μg) was placed into a headspace vial, dried overnight, and flushed with helium. 10 mL of 100 % phosphoric acid was added to each sample and allowed to react. The liberated $CO_2$ gas was measured using an EUROPA Scientific GEO 20-20 mass spectrometer fitted with a microCAPS for carbonate analysis. Results are reported in standard delta notation relative to Vienna Pee Dee Belemnite (VPDB). An in-house standard of Carrara Marble, calibrated to NBS-19 Limestone, was measured multiple times to evaluate accuracy and precision. The external analytical precision (1σ), based on these replicate analyses, was 0.028 ‰ for $\delta^{13}C$ and 0.057 ‰ for $\delta^{18}O$.

The amount of $CaCO_3$ in each sample was calculated from the beam height response during isotope mass spectrometer measurements (Spofforth et al., 2010). The liberated $CO_2$ gas, when squeezed up in the bellows, is measured and generates a current, the beam height. The pressure of $CO_2$ gas is directly proportional to the beam height and therefore the mass of carbonate in the sample. Over 100 samples of pure $CaCO_3$, with masses between 200 and 480 μg, were analyzed to establish a linear relationship between beam height and carbonate content ($CaCO_3 = mx + b$; $R^2$ = 0.94 - 0.99). Results were validated by analyzing 30 samples on a C-H-N-O elemental analyzer.

### 3.3 Calcareous nannofossils

The un-powdered sample split was examined for calcareous nannofossils. Raw sediments were processed to prepare standard smear slides (Bown and Young, 1998). To assess the reproducibility of our counting methods in every single sample, a pivotal sample was prepared 10 times by two different operators. Repeated counts of the identical sample performed by different analysts gave similar results (sd <2-5 %). Particle density estimates (Baccelle and Bosellini, 1965) were not carried out because samples have a high range in the terrigenous content (22 to 90 %). An increase or decrease of the silicoclastic component is mainly related to the major or minor efficiency of the chemical and mechanical weathering on land (Agnini et al., 2009). In the studied sediments, the variation in the amount of the terrigenous content through time has modified the density of the allochemic particle component. Consequently, calcareous nannofossil absolute abundances could not be estimated correctly using a homogeneous/constant particle density or by weighing the same amount of sediment for each smear slide. However, the scope of semi-quantitative counts performed in this study is to recognize the precise position of biostratigraphic biohorizons rather than use these data as a proxy of the paleoproductivity of taxa. Essentially, the identification of the appearance or disappearance of any given taxon is not affected by its stratigraphic abundance pattern, which obviously reduces the negative effect of the variable abundance of the silicoclastic component throughout the section. Samples were examined under a Zeiss light microscope at 1250× magnification. Calcareous nannofossils were determined using taxonomy proposed by Aubry (1984, 1988, 1989, 1990, 1999), Perch-Nielsen (1985) and Bown (2005).

A total of 200 samples were examined, providing an average time resolution of ca. 25 kyr. A preliminary qualitative estimate of the abundance and preservation state of calcareous nannofossil assemblages was performed for all samples. An initial large batch (185) was analyzed primarily to

provide biostratigraphic control for the Cicogna section, and the basic resultshave been presented by Dallanave et al. (2009). We re-checked and refined the positions of some biohorizons by examining 15 additional samples, primarily across some of the CIEs, such as B1/B2, PETM, H1 and H2, and K/X (Cramer et al., 2003). The calcareous nannofossil biostratigraphic schemes used by Dallanave et al. (2009) were those of Martini (1971) and Okada and Bukry (1980). The new zonal scheme of Agnini et al. (2014) is also used here. Biohorizon nomenclature follows that given by Agnini et al. (2014): Base (B), Base common (Bc), Top (T) and Top common (Tc).

Calcareous nannofossil biostratigraphic results are based on semi-quantitative analyses, which is based on counts of the number of specimens of selected taxa present in a prefixed area, 1 $mm^2$ or 3 long traverses (modified after Backman and Shackleton, 1983). Calcareous nannofossil paleoecological results are instead based on relative abundances of calcareous nannofossil taxa (percent of the total assemblage), calculated from counts of at least 300 specimens.

To capture changes in calcareous nannofossil assemblages we also use a statistical approach. Principal Component Analysis (PCA) was preferred to other methods, as for instance non-metric dimensional scaling (MDS) procedure for which a small number of axes are chosen prior to the analysis and the data are fitted to these dimensions (Hammer et al., 2001). However, non-metric MDS results were performed and are available as supplementary data (Figure S2). Multivariate ANalysis Of Variance (MANOVA) was carried out on our dataset to determine if significative differences are present among the three groups of samples recognized with PCA analysis.

Principal component analysis (PCA) and MANOVA were performed on the percentages of 15 subgroups using the statistical software package, PAST ver. 2.17c (Hammer et al., 2001). The former analysis is often used for examining paleontological data (e.g., Buccianti et al., 2006; Kucera and Malmgren, 1998; Watkins and Self-Trail, 1992; Thibault and Gardin, 2010; Marino et al., 2012; Bordiga et al., 2015), as it can point out hypothetical variables (components) that explain much of

284 the variance in a multidimensional data set. The first principal component accounts for the most
285 variability in any dataset examined. Each succeeding component has the highest variance possible
286 relative to the preceding components (Hammer et al., 2001). This method also increases the
287 symmetry, homoscedasticity and linearity of the data set (Aitchison, 1986). The chosen subgroups
288 were: *Chiasmolithus, Coccolithus, Ellipsolithus, Discoaster, Ericsonia, Fasciculithus, Girgisia,*
289 *Octolithus, Prinsius, Sphenolithus, Toweius, Rhomboaster/Tribrachiatus, Zyghrablithus,* reworked
290 forms, and "others".

291 **4 RESULTS**

292

293 **4.1 Carbon isotopes**

294

295 The bulk rock $\delta^{13}C$ record for the Cicogna section can be described, in a general sense, as a long-
296 term decrease of approximately 3 ‰, punctuated by a series of negative CIEs (**Figure 4**). The most
297 prominent low in $\delta^{13}C$ coincides with the CMU.

298 Previously established polarity chron boundaries and key calcareous nannofossil biohorizons at
299 the Cicogna section (Dallanave et al., 2009) provide very good stratigraphic framework. Once placed
300 onto a common time scale, in this case WO-1 (Westerhold et al., 2008), the $\delta^{13}C$ record at Cicogna
301 is fairly similar to those generated using upper Paleocene and lower Eocene marine carbonate at
302 other locations (Cramer et al., 2003; Zachos et al., 2010; Slotnick et al., 2012). This includes, for
303 example, bulk carbonate $\delta^{13}C$ records at ODP Site 1262, and DSDP Site 577 (**Figure 5**) The relatively
304 high $\delta^{13}C$ values near the base of the Cicogna section document the late stages of the PCIM, which
305 was centered within C25r (**Figure 1**). The overall drop in $\delta^{13}C$ across the section marks the long-term
306 global decrease in $\delta^{13}C$ that lasted through Chron C24n (**Figure 1**). The record contains multiple
307 negative shifts in $\delta^{13}C$. There is, however, an intriguing difference: across the Cicogna section, the

long-term 3 ‰ shift in bulk carbonate $\delta^{13}C$ values is generally offset from that in bulk carbonate $\delta^{13}C$ records at Sites 1262 and 577 by approximately -1 ‰.

The superimposed CIEs are considered to correspond to CIEs found in $\delta^{13}C$ records from elsewhere, some of which represent known or inferred hyperthermal events (Cramer et al., 2003; Lourens et al., 2005; Nicolo et al., 2007; Zachos et al., 2010; Slotnick et al., 2012). There are three pairs of CIEs below the CMU (**Figure 4**), and during the initial upper Paleocene long-term decline in $\delta^{13}C$. These correspond with the B1/B2, C1/C2 and D1/D2 CIEs documented by others (Cramer et al., 2003; Zachos et al., 2010). Notably, at Site 1262, the B1/B2 CIEs occur during middle C25n, and the C1/C2 CIEs occur at the start of C24r (**Figure 5**). The same is true at Cicogna. Interestingly, at Cicogna, the B2 and C2 CIEs show greater magnitudes than the B1 and C1 CIEs, and these paired excursions are more pronounced than at all other locations examined to date. An additional paired CIE occurs in the uppermost Paleocene (**Figure 4**). This may correlate to a fourth set of late Paleocene CIEs documented at Site 1262 (Zachos et al., 2010).

The lower Eocene portion of the $\delta^{13}C$ record at Cicogna (**Figure 4**) begins at the CMU, which marks the PETM (Giusberti et al., 2007; Dallanave et al., 2009). As at many locations, the PETM is characterized by a prominent negative CIE. The shift in $\delta^{13}C$ at Cicogna is approximately -2.5 ‰, a decrease that begins abruptly at 28.7 m and returns more gradually to near pre-excursion values by about 33 m. From approximately 33 to 54 m, the $\delta^{13}C$ curve shows a relatively smooth trend. At 54 m, a pair of CIEs begin, with the first pair having a magnitude of about 1.0 ‰. These are the H1/H2 events (Cramer et al., 2003), which occurred in the upper part of Chron C24r (Lourens et al, 2005; Zachos et al., 2010; Dickens and Backman, 2013; Dallanave et al., 2015). Above the H1/H2 CIEs, and within Chron C24n, are a series of smaller (0.4 to 0.6 ‰) CIEs. Those at approximately 60, 65 and 72 m, are correlated with the I1/I2, J and K/X events, respectively. In summary, the $\delta^{13}C$ record at Cicogna correlates with that at ODP Site 1262 (Zachos et al., 2010) and DSDP Site 577 (Dickens and

Backman, 2013) (**Figure 5**), as well as at several other locations (Cramer et al., 2003; Slotnick et al., 2012; 2015b). This is important because it enables comparison and discussion between widely separated sedimentary records within a firm temporal framework.

### 4.2 Oxygen isotopes

The $\delta^{18}O$ values range from -1.08 to -3.64 ‰ with a mean value of -1.96 ‰ and a standard deviation (1σ) of 0.50 ‰ (**Figure 4**). However, at the broad scale, $\delta^{18}O$ increases upsection, with Paleocene samples averaging -2.10 ‰ and Eocene samples averaging -1.89 ‰. This trend is noteworthy because $\delta^{18}O$ values should decrease upsection, if the composition of the $CaCO_3$ was principally reflecting rising global temperatures through the early Eocene. The 1σ of $\delta^{18}O$ values also increases upsection, being 0.33 ‰ across Paleocene samples and 0.56 ‰ across Eocene samples.

There is virtually no correlation ($r^2$ = 0.014; r=0.12) between $\delta^{18}O$ and $\delta^{13}C$ values across all samples (**Figure 6)**. However, most "short-term" CIEs do display deceases in $\delta^{18}O$ (**Figure 4**). An interval of anomalously low $\delta^{18}O$ values occurs from 39.9 m to 40.9 m, where the spatic calcite was observed.

### 4.3 Carbonate content

The $CaCO_3$ content varies between 9.4 and 77.7 % across the sample suite, with a mean value of 54.3 % and a 1σ of 8.2 % (**Figure 4**). Two important findings emerge from the $CaCO_3$ content record. First, from 39 m to 54 m, where we find limited variance in the $\delta^{13}C$ curve, $CaCO_3$ content averages 52.1 % with a 1σ of 4.9 %. Thus, while the average is similar to that calculated for the entire section, the standard deviation is much less. At Site 1262, the corresponding time interval is also

356 characterized by limited variance in $\delta^{13}C$ values and carbonate contents, the latter inferred from the
357 abundance of Fe counts in XRF scans (Zachos et al., 2010). Second, across all samples, the $CaCO_3$
358 content co-varies somewhat (r=0.29) with $\delta^{13}C$ (**Figure 6**). This is because several lows in $CaCO_3$
359 content coincide with minima in $\delta^{13}C$, as is obvious for the B1/B2, PETM and H1/H2 events (**Figure**
360 **4**).
361
362 **4.4 Calcareous nannofossils**
363
364 Calcareous nannofossils are generally abundant, diverse, and moderately well preserved. The sole
365 exception is across a 10 cm interval from 28.75 to 28.85 m, which corresponds to the onset of the
366 CIE that marks the PETM. The three samples from this interval are virtually barren of calcareous
367 nannofossils.
368 Secondary overgrowth of calcite can partially or wholly blur species-specific morphological
369 features. Such diagenetic alteration, however, only marginally influences the relative, semi-
370 quantitative andabsolute abundance of calcareous nannofossil taxa (Toffanin et al., 2013). Calcite
371 dissolution, on the other hand, can significantly affect the relative abundances of various calcareous
372 nannofossils within a given volume of sediment. This is because the removal of more dissolution
373 susceptible taxa, such as *Toweius* and holococcoliths, necessarily increases the abundance of less
374 dissolution susceptible taxa, such as discoasters (Roth and Thierstein, 1972; Adelseck et al., 1973;
375 Roth, 1983; Bornemann and Mutterlose, 2008; Toffanin et al., 2013). In general, moderate to strong
376 calcite dissolution also decreases the total abundance of calcareous nannofossils within a given
377 volume of sediment (Adelseck et al., 1973; Toffanin et al., 2011). In the Cicogna section, calcite
378 overgrowth on discoasters is the prevalent process affecting calcareous nannofossil assemblages
379 (**Plate I**). Most assemblages display high abundances (>1000 specimens/$mm^2$) and a high diversity,

which include more fragile taxa. It follows that dissolution has not severely altered most assemblages in samples from the Cicogna section. Rather, the calcareous nannofossil record is considered to represent a genuine paleoecological signal.

Nannofossil assemblages from the Cicogna section display several general trends (**Figures 7-9**). At the most basic level, there is a decrease in the total number of nannofossils (N/mm$^2$) with decreasing age. Paleocene samples average approximately 2600 specimens/mm$^2$, whereas Eocene samples above the H1/H2 events average approximately 1200 specimens/mm$^2$. This decrease in abundance broadly corresponds to a change in calcareous nannofossil composition, as supported through a series of additional observations at the Cicogna section (**Figures 7-9**):

- *Coccolithus* and *Toweius* constitute nearly half of the assemblages considering the entire section. However, these genera show a clear decrease in abundance upsection, with a mean value of 60 % in Paleocene samples and 35 % in Eocene samples;
- *Zyghrablithus bijugatus* shows a low mean value of approximately 4 % in the Paleocene, followed by a sharp increase in the basal part of the Eocene, and a mean value of approximately 25 % upsection in the Eocene. Hence, the abundance of this taxon expands on behalf of *Coccolithus* and *Toweius*;
- *Sphenolithus* decreases progressively during the Paleocene, suddenly disappears at the onset of the PETM, before returning to and exceeding pre-PETM values in the lower Eocene. Thus, the abundance of sphenoliths also expands on behalf of *Coccolithus* and *Toweius*;
- *Fasciculithus* shows a severe decline in abundance and species diversity at the onset of the PETM (28.70 m), leading up to their extinction at 34.73 m;
- *Octolithus* is rare throughout most of the studied section, but displays high abundances from approximately 14.7 m to 27.5 m in the upper Paleocene;

- *Discoaster* does not show any distinct change in abundance except for a single peak at the onset of the PETM;
- Several Cretaceous and early Paleocene species constitute minor reworked components throughout the section. Notably, the intervals marked by the PETM, H1/H2 and, to a lesser extent, B1/B2 CIEs are characterized by higher abundances of these reworked components;
- Representatives of placolith genera, such as *Prinsius, Ericsonia, Chiasmolithus* and *Girgisia*, are minor components of most samples. *Prinsius* displays a marked permanent decrease in abundance from a mean value of approximately 6 % to 2.5 % across the Paleocene/Eocene boundary. By contrast, *Ericsonia* does not show a prominent difference in abundance between Paleocene and Eocene assemblages, but increases in abundance during known and suspected hyperthermal events;
- The Calcareous Nannofossil Excursion Taxa (CNET), which include *Discoaster araneus* and the genus *Rhomboaster* are present during the CIE of the PETM. The evolution of the *Rhomboaster*/*Tribrachiatus* plexus started at the onset of the PETM, when *Rhomboaster* and *T. bramlettei* first appeared, and continued into the lower Eocene with the successive appearances of *T. contortus* and *T. orthostylus* (Raffi et al., 2005; Agnini et al., 2006; 2007b).

Beyond the above variations, evolutionary appearances and extinctions occur during the studied time interval (**Figures 7-9**). Most of these species belong to *Discoaster, Sphenolithus* and the *Rhomboaster/Tribrachiatus* lineage, and include *D. multiradiatus, D. diastypus, D. lodoensis, S. radians, S. anarrhopus, T. bramlettei, T. contortus* and *T. orthostylus*. The biohorizons defined using these species are exceptionally useful for biostratigraphy and, interestingly, often occur close to changes in $\delta^{13}C$.

All assemblage data were used for PCA analysis. This indicates that PC1 (41.3 %) and PC2 (14.7 %) together account for 56 % of the variance in the dataset. The PCA graph (**Figure 10A; Figure S1**

**supporting material**) shows that samples can be subdivided into three subgroups. The first two populations of samples are distinguished because of their different positions along the x-axis (PC1). The third population is much more dispersed but a possible discrimination from the other two seems to be hypothesized because of its different position along the y-axis (PC2). The use of a different statistical procedure, as for instance MDS, does not substantially change these results (**Figure S2**). To further support the subdivision of the study samples in three subgroup, we applied the MANOVA analysis to our data set (Figure 10B). The result clearly confirmed that that Paleocene, PETM and Eocene samples are in fact isolated one from each other.

## 5 DISCUSSION

### 5.1 Integrated stratigraphy and a carbon isotope template

Polarity chron boundaries and calcareous nannofossil biohorizons (**Table 1; Figure 4**) provide a solid stratigraphic framework for the Cicogna section. Calcareous nannofossil biohorizons, including additional ones defined here, align in same stratigraphic order when compared to other locations, such as ODP Site 1262 and DSDP Site 577 (**Table 1; Figure 11**). The Cicogna section represents sediment accumulation between 57.5 and 52.2 Ma on the WO-1 time scale (Dallanave et al., 2009). The average SR was ca.15.2 m/Myr, although this must have varied (**Figures 3, 11**). The CMU, which marks the "core" of the PETM and ca. 80-100 kyr, showing a higher sedimentation rate than much of the remaining record (Dallanave et al., 2009; Krishnan et al., 2015).

Once placed into the above stratigraphic framework, the bulk carbonate $\delta^{13}C$ profile documented at Cicogna correlates well to that generated at ODP Site 1262 (**Figure 5**). In fact, it is similar to $\delta^{13}C$ profiles generated at multiple locations (**Figure 2, Figure S4**), as long as records have

been properly calibrated in both the depth and time domains. This includes accounting for core stretching and core gaps at scientific drilling sites, such as at DSDP Site 577 (Dickens and Backman, 2013), and accounting for changing strike and dip along land sections, such as done at Cicogna (**Figure 3**). During late Paleocene and early Eocene times, the Cicogna section records the long-term decrease in $\delta^{13}C$. Superimposed on this drop were multiple, often paired, negative CIEs. The PETM definitively represents the most prominent CIE, but several other CIEs occurred before and after. Importantly, the relative positions of polarity chron boundaries, key calcareous nannofossil biohorizons and CIEs at Cicogna align well with those found at other locations (**Table 1**; **Figures 5, 11**).

A clearly recognizable $\delta^{13}C$ pattern spans the late Paleocene through the early Eocene at several locations (Cramer et al., 2003; Nicolo et al., 2007; Galeotti et al., 2010; Zachos et al., 2010; Slotnick et al., 2012, 2015b), although the total number of CIEs remains uncertain. At Cicogna, the problem lies in the interval surrounding the K/X event, which broadly corresponds to the start of the EECO (see discussion in Slotnick et al., 2012). We cannot confirm with our sample resolution whether a series of short-term, small amplitude CIEs mark this time, an idea suggested from $\delta^{13}C$ records of the Clarence Valley sections (Slotnick et al., 2012; 2015b). However, as at other locations, such as Site 1262, no significant CIEs occurred within the 1.6 Myrs between the PETM and the H-1/ETM-2 event (**Figure 5**).

The time-correlative $\delta^{13}C$ template implies changes in the mean ocean $\delta^{13}C$ of dissolved inorganic carbon (DIC). In turn, these compositional changes very likely represent variations in fluxes of highly $^{13}C$-depleted carbon to and from the ocean or atmosphere, such as changes in the release and storage of organic carbon (Shackleton, 1986; Dickens et al., 1997; Kurtz et al., 2003; Deconto et al., 2010; Komar et al., 2013). The $\delta^{13}C$ record at Cicogna offers no direct insight on the location of this carbon (e.g., seafloor methane, permafrost, peat). However, it does support an important

475 concept: the magnitudes of given CIEs appear somewhat related to one another and to the long-
476 term $\delta^{13}C$ record. In particular, the PETM occurred about halfway between the long-term high and
477 low in $\delta^{13}C$, and heralded a relatively long time interval lacking CIEs. A generic explanation is that a
478 very large mass of $^{13}C$-depleted carbon was injected from some organic reservoir into the ocean or
479 atmosphere during the PETM, and that the reservoir needed to recharge for considerable time
480 before the next injection (H-1/ETM-2) could occur (Dickens et al., 2003; Kurtz et al., 2003; Lunt et
481 al., 2011; Komar et al., 2013).

482 The overall -1 ‰ offset of the $\delta^{13}C$ curve between the records at Cicogna and at Sites 577 and
483 1262 (**Figure 5**) warrants brief discussion. It probably does not reflect wholesale diagenesis and
484 resetting of the primary signal at any of these sections. Otherwise, a recognizable correlative $\delta^{13}C$
485 record and well-preserved nannofossils (**Plate I**) would not be found at all three locations. In fact, it
486 is difficult to modify the original $\delta^{13}C$ composition of carbonate over appreciable distance (> than
487 several meters) in marine sedimentary sequences dominated by fine grained calcite, even those
488 now exposed on land as lithified rock, such as at Cicogna or in the Clarence Valley. This is because
489 the carbon water/rock ratio remains low, because almost all carbon exists in carbonate, and because
490 temperature minimally influences carbon isotope fractionation (Matter et al., 1977; Scholle and
491 Arthur, 1980; Frank et al., 1999). Instead, the offset in the $\delta^{13}C$ curves probably relates to differences
492 in the composition of the original carbonate, a concept that we return to later.

493 However, local dissolution and re-precipitation of carbonate definitely has occurred in the
494 Cicogna section. This can be observed in the overgrowths of secondary calcite on discoasters and
495 *Rhomboaster/Tribrachiatus* (**Plate I**). This process should dampen the original CIEs, because on the
496 meter-scale, dissolution and re-precipitation of carbonate would involve $\delta^{13}C$ gradients in the DIC
497 of surrounding pore water (Matter et al., 1977; Scholle and Arthur, 1980). This may explain, in part,

why the magnitude of early PaleogeneCIEs in bulk carbonate records are often muted relative to those found in other carbon-bearing phases (Slotnick et al., 2015b).

### 5.2 Oxygen isotopes and a problem recording past temperatures

The $\delta^{18}O$ record at Cicogna is intriguing because many of the CIEs are characterized by negative excursions but absolute values of $\delta^{18}O$ generally and unexpectedly increase upsection (**Figure 4**). Similar results have been documented in bulk carbonate stable isotope records at other locations, such as ODP Site 1215 (Leon-Rodriguez and Dickens, 2010) and Mead Stream (Slotnick et al., 2012). Even the $\delta^{18}O$ record of bulk carbonate at Site 1262 shows minimal long-term change from the late Paleocene to the early Eocene (Zachos et al., 2010), the time when high-latitude surface temperatures and deep ocean temperatures presumably increased by 5-6 °C, and one might expect a >1 ‰ decrease in the $\delta^{18}O$ of marine carbonate.

Like previous workers, we cannot discount the notion that temperatures at low and high latitudes responded differently across the early Paleogene (Pearson et al., 2007; Huber and Caballero, 2011). Unlike for carbon isotopes, however, local dissolution and re-precipitation of carbonate should significantly impact the $\delta^{18}O$ of marine carbonate. This is because the oxygen water/rock ratio would be high before lithification, and because temperature strongly influences oxygen isotope fractionation (Matter et al., 1975; Scholle and Arthur, 1980; Frank et al., 1999). In general, as calcite-rich sediments and surrounding pore water are buried to higher temperatures along a geothermal gradient, local dissolution and re-precipitation of carbonate shifts carbonate $\delta^{18}O$ to lower values (above references; Schrag et al., 1995). It is likely that, during sediment burial, the bulk carbonate $\delta^{18}O$ records in many lower Paleogene sections, including at Cicogna, have been modified. We suggest that a signal of surface ocean temperature changes remains in the Cicogna

522 section, which gives rise to short-term $\delta^{18}O$ excursions that coincide with CIEs and several known or
523 suspected hyperthermal events. However, the entire $\delta^{18}O$ record at this location likely has shifted
524 to more negative values preferentially with increasing burial depth and age. This partly explains the
525 observed relationship between bulk carbonate $\delta^{13}C$ and $\delta^{18}O$, which lies along a trajectory expected
526 for diagenesis (**Figure 6**). A potential test of this idea would be to show that the overgrowths on
527 nannofossils (**Plate I**) have a significantly lower $\delta^{18}O$ than the primary core carbonate of nannofossil
528 tests.
529
530 **5.3 Calcareous nannofossil assemblages within the context of correlative stable isotope records**
531
532 A detailed stable carbon isotope curve provides a powerful tool to place past changes in calcareous
533 nannofossil assemblages into a highly resolved framework. This is because, as implied above, truly
534 global changes in the $\delta^{13}C$ composition of the ocean should occur within the cycling time of carbon
535 through ocean, which is <2000 years at present-day and presumably for the entire Cenozoic
536 (Broecker and Peng, 1982; Shackleton, 1986; Dickens et al., 1997).
537 Across the study interval at Cicogna, several calcareous nannofossil taxa appear or disappear
538 (**Table 1**). Moreover, their abundances also change between these horizons (**Figures 7-9**). One might
539 hypothesize that these changes in nannofossil assemblages were related to the established (e.g.,
540 the PETM, H1/ETM-2 and K/X) and potential (e.g., the B1/B2, I1/I2) hyperthermal events that
541 occurred during the late Paleocene and early Eocene (**Figures 1, 5**). However, the timing between
542 recorded evolutionary appearances and extinctions of calcareous nannofossils and perturbations in
543 $\delta^{13}C$ are variable (**Figures 7-9**). For instance, several significant calcareous nannofossil changes
544 observed close to H1/H2 hyperthermals (e.g., B *T. othostylus*, B *S. radians*, B *S. villae*, Tc *D.*
545 *multiradiatus,* T *T. contortus*) predate these events. By contrast, several biotic changes observed

546 close to the B1/B2 CIEs (e.g., B *D. delicatus,* Tc *S. anarrhopus,* B *D. multiradiatus*, T *Ericsonia robusta*)
547 happened at the end of these events. The PETM seems to provide the only case when a negative
548 CIE precisely corresponds to major changes in calcareous nannofossil assemblages.
549 Profound changes in calcareous nannofossil assemblages occurred across the PETM in several
550 locations (**Figure 2**), both in terms of relative abundances and increases in origination and extinction
551 rates (Aubry, 1998; Bown et al., 2004; Raffi et al., 2005; Gibbs et al., 2006a; Agnini et al., 2007a; Self-
552 Trail et al., 2012). At Cicogna, the assemblages show remarkable, though mostly transient, relative
553 abundance variations across the PETM, including an increase in *Coccolithus*, a decrease in
554 *Zygrhablithus, Sphenolithus, Toweius* and *Prinsius*, and an extinction of most fasciculith species
555 (**Figure 8**). Not surprisingly, these changes are very similar to those in the Forada section, which is
556 also located in the Belluno Basin (Agnini et al., 2007a).
557 Although these changes in relative abundance of taxa alone represent a notable difference with
558 respect to background conditions, most of the changes are transient and/or local when compared
559 with other datasets (Bralower, 2002; Gibbs et al., 2006b; Agnini et al., 2007b; Angori et al., 2007;
560 Mutterlose et al., 2007). For instance, an increase in abundance of *Discoaster* and *Fasciculithus* was
561 reported for some of the PETM section studied (e.g., Bralower, 2002; Tremolada and Bralower,
562 2004; Raffi et al. 2009), but these assemblage variations were not observed in other sections (e.g.,
563 Gibbs et al. 2006; Agnini et al., 2007a; Self-Trail et al., 2012). The only global calcareous nannofossil
564 assemblage features of the PETM are represented by the evolutionary appearance of
565 *Rhomboaster/Tribrachiatus* lineage, the presence during the CIE of short-lived species such as
566 *Discoaster areneus*, and the disappearance of several species of fasciculiths (Raffi et al., 2005; Agnini
567 et al., 2007a).
568 While changes in calcareous nannoplankton assemblages during the PETM have been
569 investigated at high resolution at different locations (e.g., Bralower, 2002, Gibbs et al., 2006b; Agnini

et al. 2007a), the longer-term perspective in which such changes occurred during the early Paleogene has remained uncertain (Gibbs et al., 2012). The record at Cicogna provides this opportunity.

The PCA analysis of calcareous nannofossil census data (%) indicates that two principal components (PC1 and PC2) account for most (56.0 %) of the variability in our 15 selected subgroups. Such analysis also permits the studied samples to be subdivided into two populations and a possible widely dispersed group (**Figure 10A**). The first two populations are distinguished because of a major difference along the x-axis representing PC1, whereas the third population seems to stand out because of a difference along the y-axis representing PC2. Importantly, each of these three populations constitutes a homogeneous group in the time domain: Group 1 includes all upper Paleocene samples (Paleocene samples and B1/B2 events); Group 2 consists of almost all lower Eocene samples (Eocene samples, H1/H2 events and K event); Group 3 comprises samples that span the PETM (both core and recovery), and two samples that come from sediment deposited during the core of the H1 and B2 events (**Figure 10**). These results indicate that late Paleocene calcareous nannofossil assemblages are statistically different in their composition from those of early Eocene samples. To check if calcareous nannofossil assemblages across the PETMare statistically different from those of either the late Paleocene or the early Eocene, we performed a MANOVA analysis, which pointed out that ellipses containing 95%of the data points for each group (late Paleocene, early Eocene and PETM) are virtually not overlapping one to each other suggesting that three statistically different populations are recognized across the PETM, the late Paleocene and the early Eocene background assemblages, and the PETM fossil associations.

The general shift in the relative abundance of placoliths (i.e., *Coccolithus, Toweius* and *Prinsius*), the major component of the late Paleocene assemblages, to nannoliths/holococcoliths (i.e.,

*Sphenolithus* and *Zygrhablithus*), the major component of the early Eocene assemblages, largely explains the PC1 component or Axis 1 (Figure 10). By contrast, the dramatic shift toward negative values in the PC2 component or Axis 2 during the PETM happens because of the increase of *Ericsonia* and reworking and the presence of *Rhomboaster-Tribrachiatus* plexus. Presumably, this relates to peculiar paleoenviromental conditions that developed during the event. One can hypothesize that this may have been a major difference in the physicochemical parameters of sea surface waters, such as higher temperatures, higher nutrient concentration or reduced carbonate saturation state.

Statistical analysis of our data from Cicogna does not highlight any prominent short-term changes in calcareous nannofossil assemblages, other than across the PETM and perhaps the B2 and H1 events. However, several biohorizons occur around the B1/B2 events. Specifically, these are the Bc *Z. bijugatus*, the brief high abundance of *Octolithus* spp., the evolutionary onset of the *D. delicatus/D. multiradiatus* lineage, the presence of the short-ranged *E. robusta*, the final radiation of late Paleocene fasciculiths (i.e., *F. richardii* group, *F. hayi, F. lilianae, F. alanii*), and the Tc of *S. anarrhopus*. All these happened at Cicogna and at Site 1262 within Chron C25n (Agnini et al., 2007b; Dallanave et al., 2009; **Figure 11)**, which spanned only 0.54 Myr (Westerhold et al., 2008). These near-synchronous events are intriguing because while the various nannofossils represent only minor components of late Paleogene assemblages, they were destined to become either an abundant constituent of Eocene populations (e.g., *Z. bijugatus* and the *D. delicatus/D. multiradiatus* lineage), or extinct after having been a distinctive element of Paleocene assemblages (e.g. *Fasciculithus* spp. and *S. anarrhopus)*. Following the PCIM, the long-term increase in temperature and decrease in $\delta^{13}C$ (**Figure 1**) coincided with a series of minor changes in nannofossil assemblages, which subsequently became important, presumably for evolutionary reasons.

Similar to the late Paleocene, calcareous nannofossil assemblages after the PETM do not show major rearrangements of common taxa during the early Eocene. Instead, minor components of

618 these assemblages exhibit a sequence of closely spaced biohorizons. The sequence of these
619 biohorizons is: T *Fasciculithus,* B *D. diastypus*, B *T. contortus,* T *T. bramlettei*, Tc *D. multiradiatus,* T
620 *T. contortus*, B *T. orthostylus,* B *S. radians,* T *D. multiradiatus,* B *D. lodoensis,* B *G. gammation* and
621 Bc *D. lodoensis* (**Table 1**). Within the resolution of available paleomagnetic and $\delta^{13}C$ data, all these
622 biohorizons are virtually synchronous between the Cicogna section and ODP Site 1262 (**Figure 11**).
623 They also almost all occurred in near synchrony at Site 577 (Dickens and Backman, 2013), although
624 the precise correlation remains uncertain, given problems with coring disturbance and subtleties in
625 age models at this location.
626 Importantly, for stratigraphic purposes, the B and Bc of *D. lodoensis* are approximately coeval
627 at all three locations and spaced apart by about 750 kyr. Unless one examines samples in detail,
628 these two biohorizons can be confused and result in an erroneous assignment of early Eocene ages.
629 The evolutionary appearances and extinctions amongst early Eocene nannofossil assemblages
630 may suggest the presence of uneven communities living in an extreme climate in which alterations
631 of environmental conditions, even minor, might trigger evolutionary changes or prominent
632 variations in abundances of a limited number of taxa that typically do not represent the dominant
633 component of assemblages. explained possible explanation is a generally higher tolerance of
634 cosmopolitan taxa to variations in environmental conditions (Boucot, 1975; Winter et al., 1994). In
635 contrast, highly specialized taxa that are adapted to a particular ecological niche, may display
636 greater sensitivity to modifications in the photic zone environment (MacArthur and Wilson, 1967;
637 Pianka, 1970; Baumann et al., 2005).
638 In summary, several genera of calcareous nannofossils, such as *Rhomboaster, Tribrachiatus,*
639 *Sphenolithus, Discoaster* and *Zygrhablithus* were, at least to some extent, affected during the late
640 Paleocene-early Eocene transition, because they show an increased rate of taxonomic evolution
641 (**Figure 11**). However these genera are all minor groups in terms of overall abundance, at least in

642 most lower Paleogene sediment sequences, and they all belong to nannoliths and holococcoliths. It
643 appears that these organisms were more sensitive to environmental changes than heterococcoliths,
644 for example the cosmopolitan genera *Coccolithus* and *Toweius*.
645
646 **5.4 Early Paleogene calcareous nannofossil evolution**
647
648 Any comprehensive paleoenvironmental interpretation involving early Paleogene calcareous
649 nannofossils remains tentative because many taxa, such as *Rhomboaster*/*Tribrachiatus*, *Discoaster,*
650 *Sphenolithus* and *Zygrhablithus*, are extinct. Still, some single species or species groups are
651 considered to be useful for reconstructions of paleoenvironmental conditions (Geisen et al., 2004).
652 With that viewpoint, and with an understanding of modern holococcolith/nannolith ecology and
653 classical biogeographical model, we provide a scenario regarding late Paleocene-early Eocene
654 calcareous nannofossil evolution.
655 Modern holococcolithophores have numerous tiny rhombohedral calcite crystallites, and are
656 considered as haploid stages of certain heterococcolithophores, which can live in just about any
657 marine photic zone environment, although higher abundances and diversity are typical in
658 oligotrophic settings (Billard and Inouye, 2004). The most common Paleogene holococcolith was
659 *Zygrhablithus bijugatus.* This taxon has been interpreted as a *K*-specialist more adapted to stable
660 environments and oligotrophic conditions (Aubry, 1998; Bralower, 2002; Tremolada and Bralower,
661 2004; Agnini et al., 2007a; Self-Trail et al., 2012). Nannolith is a term used to describe peculiar
662 morphotypes usually observed in association with coccoliths, but lacking the typical features of
663 heterococcoliths or holococcoliths. *Ceratolithus cristatus,* a modern nannolith, has been observed
664 on the same cell together with *Neosphaera coccolithomorpha* (Alcolber and Jordan, 1997),
665 suggesting that the nannolith stage (*C. cristatus*) corresponds to the holococcolith stage in other

taxa (Young et al., 2005). Paleogene nannoliths include taxa with peculiar morphologies such as *Discoaster, Fasciculithus* and *Sphenolithus*. These genera often have been associated with warm waters and oligotrophic environments and are almost unanimously interpreted as *K*-specialists (Haq and Lohmann, 1976; Backman, 1986; Wei and Wise, 1990; Bralower, 2002; Gibbs et al., 2004; 2006a; 2006b; Agnini et al., 2007a). *K* specialists fluctuate at or near the carrying capacity (K) of the environment in which they thrive (MacArthur and Wilson, 1967), and are usually characterized by long individual life-cycles and low reproductive potential. The *K*-specialist strategy is advantageous in highly stable, typically oligotrophic environments, which allows the evolution of stenotopy and where organisms compete by specialization and habitat partitioning (Hallock, 1987; Premoli Silva and Sliter, 1999). The narrow range of adaptability to changes in habitat or ecological conditions stimulates a rapid speciation.

At present, it is commonly accepted that modern holococcoliths and nannoliths are not produced by autonomous organisms; rather, they are stages in the life cycle of coccolithophores., Moreover, the passage between the two stages may be triggered by environmental factors (Billard and Inouye, 2004).

Hence, though Paleogene holococcoliths/nannoliths have no direct descendants in present-day oceans, they may very well have shared similar physiological features and life cycles with modern taxa. Assuming this is the case, the increase in the relative abundance of holococcoliths and nannoliths at the expense of heterococcoliths as well as the higher rates of evolution shown by holococcoliths and nannoliths may suggest conditions in which highly specialized taxa could flourish and rapidly evolve. This scenario is consistent with the idea, based on laboratory and modern ocean data, that the calcareous nannoplankton response to environmental change is species or group specific rather than homogeneous across the entire assemblage (Riebesell et al., 2000; Langer et al., 2006; Iglesias-Rodriguez et al., 2008; Lohbeck et al., 2012). Variations in the thermal and chemical

690 structure of photic zone waters may thus account for the observed changes in the early Paleogene
691 calcareous nannofossil assemblages.
692
693 **5.5 Carbon isotope of surface waters during the early Paleogene**
694
695 Like at Cicogna, well-preserved calcareous nannofossils dominate bulk sediment carbonate contents
696 of early Paleogene strata at Sites 577 and 1262 (Backman, 1986; Zachos et al., 2004; Dickens and
697 Backman, 2013). Given that the nannofossil assemblages are fairly similar (**Figure 11**), a really basic
698 question returns: why is the overall early Paleogene bulk carbonate $\delta^{13}C$ record at Cicogna less by
699 approximately 1 ‰?
700 A variety of explanations for the $\delta^{13}C$ offset can be offered. For example, sediments at Cicogna had
701 greater amounts of organic matter, and during burial diagenesis, a fraction of this carbon was
702 consistently added so as to decrease the $\delta^{13}C$ of pore water DIC. We note, though, that $C_{org}$ contents
703 (wt %) at the proximal Forada section generally have values less than 0.1 wt % (Giusberti et al.,
704 2007). Similar $C_{org}$ contents are found at ODP Site 1262, where values range from 0.0 to 0.3 wt %
705 (Zachos et al., 2004).
706 A cursory examination of early Paleogene bulk carbonate $\delta^{13}C$ records from other sites of the
707 North Atlantic/western Tethys region (e.g., Sites 550 and 1051; **Figure 2**) shows a commonality:
708 these locations also display negative 0.5 to 1 ‰ offsets relative to correlative records at Sites 577
709 and 1262 (Cramer et al., 2003). The $\delta^{13}C$ of DIC in modern surface waters (<100 m) ranges by about
710 2 ‰, because of the differences in temperature, primary productivity and water mass mixing
711 (Kroopnick, 1985; Tagliabue and Bopp, 2008). Notably, however, gradients in $\delta^{13}C$ of surface water
712 DIC are gradual, such that large regions have fairly similar values. It is possible that bulk carbonate

713 $\delta^{13}C$ values in early Paleogene North Atlantic sections record lower values than locations near the
714 Equator or in southern latitudes because of past ocean circulation.
715
716 **6 SUMMARY AND CONCLUSIONS**
717
718 We generate records of bulk carbonate $\delta^{13}C$ and $\delta^{18}O$, $CaCO_3$ content and calcareous nannofossil
719 assemblages from the Cicogna section, a marine sedimentary succession that now crops out along
720 a stream in the Southern Alps of northeast Italy. The combined geochemical and calcareous
721 nannofossil results allow us to generate a detailed stratigraphy for the section, as well as to explore
722 relationships between stable isotope variations and nannofossil assemblages. Most lower
723 Paleogene sections examined to date lack such coupled data sets.
724 The $\delta^{13}C$ record and calcareous nannofossil assemblages show that the section spans ~5.3 Myr
725 of the late Paleocene and early Eocene interval, from 57.5 to 52.2 Ma on the WO-1 timescale. This
726 is consistent with previous paleomagnetic information and preliminary calcareous nannofossil
727 biostratigraphy (Dallanave et al., 2009), but provides a more detailed stratigraphic framework, one
728 appropriate for correlations to other locations around the world. In particular, the fairly well
729 resolved $\delta^{13}C$ record shows long-term and short variations that correspond to those found in several
730 other sections, including an established series of negative CIEs. The most prominent CIE marks the
731 PETM, while other less pronounced CIEs represent the H-1, K/X and other "events" documented
732 elsewhere. The $\delta^{13}C$ variations observed at Cicogna clearly reflect global changes in the fluxes of
733 carbon to and from the ocean and atmosphere.
734 PCA analysis of calcareous nannofossil assemblages shows three distinct sample clusters. Late
735 Paleocene and early Eocene assemblages were distinctly different from each other and from that of
736 the PETM. Indeed, the PETM, the most intense hyperthermal during the late Paleocene - early

737 Eocene, was characterized by a unique calcareous nannofossil assemblage composition. This
738 suggests that the brief episode of extreme warming permanently modified the composition of
739 calcareous nannoplankton through an increase in the rate of taxonomic evolution (Gibbs et al.,
740 2006a). Less prominent hyperthermal events do not show significant variations in the main
741 components of assemblages, but rather were characterized by a series of changes affecting a limited
742 number of rare taxa. These taxa may have been less tolerant to environmental changes in their
743 habitats.

744 More common taxa, essentially consisting of placoliths, such as the cosmopolitan *Coccolithus*
745 and *Toweius*, display a progressive long-term decrease interrupted by transient changes in their
746 relative abundance but virtually no extinction or origination events occur in these groups during the
747 pertinent time interval. Species belonging to nannoliths and holococcoliths (*Discoaster,*
748 *Fasciculithus, Rhomboaster/Tribrachiatus, Sphenolithus* and *Zygrhablithus*), generally show a higher
749 rate of evolution and a higher concentration of biohorizons close to $\delta^{13}C$ perturbations. In
750 conclusion, calcareous nannoplankton show a different response of the various components of the
751 assemblages, this is consistent with a species or taxonomic unit sensitivity of calcareous
752 phytoplankton to paleoenviromental perturbations. This evolutionary climate-forced model is
753 supported by data from ODP Site 1262, which demonstrate that these changes are global and
754 synchronous between middle latitudes in the western Tethys region and the South Atlantic.

755

756 **7 ACKNOWLEDGMENTS**

757 CA would like to thank Carlotta Betto for preparing smear slides for calcareous nannofossil
758 analyses. We also acknowledge valuable comments from the referees two anonymous reviewers.
759 Funding for this work came from several sources. Primary support came from a MIUR grant to CA,
760 ED and DR (PRIN 2010-2011 - prot. 2010X3PP8J_003. JB acknowledges support from the Swedish

761 Research Council. GRD received funding from a National Science Foundation (NSF) grant (NSF-
762 FESD-OCE-1338842).

## 8 FIGURE AND TABLE CAPTIONS

**Figure 1**. Middle Paleocene to middle Eocene (64 to 48 Ma) stable isotope ($\delta^{13}C$ and $\delta^{18}O$) records of benthic foraminifera from multiple locations (Zachos et al., 2008) placed on the Option 1 (W01) time scale of Westerhold et al. (2008). Also shown are positions of polarity chrons and calcareous nannofossil biozones for this time interval, both from the CP Biozone scheme (Okada and Bukry, 1980) and the CN Biozone scheme (Agnini et al., 2014). Various "events" are noted within this chronostratigraphic framework, including the Paleocene carbon isotope maximum (PCIM), the Paleocene-Eocene thermal maximum (PETM), the H-1/ETM-2 event, the K/X event, and the Early Eocene Climatic Optimum (EECO). To the right is the general lithologic column and magnetostratigraphy of the Cicogna section (Dallanave et al., 2009).

**Figure 2.** Paleogeographic map indicating approximate locations at 55 Ma for several key sites with detailed stable isotope records across the late Paleocene and early Eocene. These include (marked with black dots and star) the Cicogna section (NE Italy, this study), DSDP Site 577 (Shatsky Rise, Dickens and Backman, 2013), ODP Sites 1051 (Blake Nose, Ogg and Bardot, 2001), 1215 (central Pacific, Raffi et al., 2005), and 1262 (Walvis Ridge, Westerhold et al., 2008), and the Clarence Valley (CV) sections (New Zealand, Slotnick et al., 2015b). The grey areas represent plate fragments, while the black lines show present-day shorelines. Boxes next to site locations show average sedimentation rates from the base of Chron C25n to the base of Chron C23r (57.20 - 52.36 Ma). The base map is from http://www.odsn.de/odsn/services/paleomap/paleomap.html. Red triangles are locations where a decrease in diversity of *Fasciculithus* spp. has been documented near the PETM. Locations include the Clarence Valley sections, central Pacific (ODP Sites 1215, 1220, 1221), western Pacific (DSDP Site 577 and ODP Site 865), South Atlantic (Walvis Ridge, DSDP Site 527, ODP Sites 1262,1263-1267; Maud Rise, ODP Site 690), equatorial Atlantic (Ceara Rise, ODP Site 929, Demerara

787 Rise, ODP Sites 1259, 1260), northwestern Atlantic (New Jersey Margin land sections, ODP Site 1051,
788 IODP Site U1403, U1409), northeastern Atlantic (Bay of Biscay DSDP Sites 401, 549 and 550, Zumaya
789 land section), Indian Ocean (DSDP Site 213; ODP 672; Kerguelen Plateau, ODP Site 1135)(Backman,
790 1986; Aubry, 1999; Bralower, 2002; Dupuis et al., 2003; Tremolada and Bralower, 2004; Bralower
791 and Mutterlose, 1995; Monechi et al., 2000; Gibbs et al., 2004; Raffi et al., 2005; Agnini et al., 2007a;
792 Angori et al., 2007, Mutterlose et al., 2007; Jiang and Wise, 2009; Shamrock, 2010; Norris et al, 2014;
793 Dallanave et al., 2015).
794
795 **Figure 3**. The location and representative photographs of the Cicogna section in northeast Italy. (a)
796 Geographic map showing the main Late Cretaceous–early Paleogene paleogeographic domains of
797 the Italian Southern Alps (modified after Cati et al., 1989); (b) Geological map of the local area
798 (modified after Costa et al, 1996 indicating also the location of the Cicogna section (red asterisk); (c)
799 Alternating beds of Paleocene gray-green marls and calcareous marls (0-20 m); (d) The Scaglia Rossa
800 *sensu latu* overlain by the Belluno Flysch; (e) Marl/calcareous marl couplets in the lower Eocene
801 portion of the section (approximately 40.0-70.0 m); (f) The base of the Clay Marl Unit, which denotes
802 the onset of the PETM (approximately 28.7-29.3 m); (g) The brownish-red interval of clayey marls
803 with sporadic grey-green cm-scale spots and lenses, the CMU, overlain by prominent rhythmic
804 alternations of marls and calcareous marls ( approximately 28.7-33.0 m).
805
806 **Figure 4.** The Cicogna section with records of bulk carbonate $\delta^{13}C$ and $\delta^{18}O$ data, and $CaCO_3$ content.
807 Calcareous nannofossil biostratigraphy (CP and NP biozones) and magnetostratigraphy are after
808 Dallanave et al. (2009), CN biozones are also reported. Orange and yellow bands mark major $\delta^{13}C$
809 excursions. Dashed lines indicate minor CIEs that have been labeled elsewhere (e.g., E1/E2, F and

G; Cramer et al., 2003), whereas dotted lines indicate minor changes in $\delta^{13}C$ that appear to occur also at ODP Site 1262 (see also **Figure 5**).

**Figure 5.** Stratigraphic correlation between upper Paleocene and lower Eocene sections at Cicogna, ODP Site 1262 (Zachos et al., 2010), and DSDP Site 577 (Cramer et al., 2003; Dickens and Backman, 2013). All three sites have independently derived nannofossil biohorizons, polarity chrons and $\delta^{13}C$ records, which account for subtle temporal offsets. . Color bands and symbols are the same as in Figure 4. Note the missing record at Site 577 that corresponds with known core gaps.

**Figure 6.** Plots of (a) bulk carbonate $\delta^{13}C$ versus bulk oxygen$\delta^{18}O$, and (b) bulk carbonate $\delta^{13}C$ versus $CaCO_3$ contentfor samples from the Cicogna section. The black arrow shows the expected effect of burial diagenesis. Grey and black dash lines are linear trendlines for Paleocene and Eocene samples, respectively. Note the clear distinction in $\delta^{13}C$ for Paleocene and Eocene samples, which relates to a long-term decrease in $\delta^{13}C$ (**Figure 5**).

**Figure 7.** Relative (%) and semi-quantitative ($N/mm^2$) abundances of selected calcareous nannofossil genera across the Cicogna section. Also shown are the lithostratigraphy, magnetostratigraphy, biostratigraphy and carbon isotope ($\delta^{13}C$) stratigraphy at the Cicogna section (**Figure 4**). Color bands and symbols are the same as in previous figures.

**Figure 8.** Relative (%) and semi-quantitative ($N/mm^2$) abundances of selected, mainly late Paleocene, calcareous nannofossil taxa across the Cicogna section. Also shown are the lithostratigraphy, magnetostratigraphy, biostratigraphy and carbon isotope ($\delta^{13}C$) stratigraphy at the Cicogna section (**Figure 4**). Color bands and symbols are the same as in previous figures.

834 **Figure 9.** Relative (%) and semi-quantitative (N/mm$^2$) abundances of selected, mainly early Eocene,
835 calcareous nannofossil taxa across the Cicogna section. Also shown are the lithostratigraphy,
836 magnetostratigraphy, biostratigraphy and carbon isotope ($\delta^{13}C$) stratigraphy at the Cicogna section
837 (**Figure 4**). Color bands and symbols are the same as in previous figures.
838
839 **Figure 10.** Statistical Analyses of calcareous nannofossil percentage data of the Cicogna section.
840 Calcareous nannofossils are subdivided into 15 subgroups (*Chiasmolithus, Coccolithus, Ellipsolithus,*
841 *Discoaster, Ericsonia, Fasciculithus, Girgisia, Octolithus, Prinsius, Sphenolithus, Toweius,*
842 *Rhomboaster/Tribrachiatus, Zyghrablithus*, reworking, others). **A)** Principal Component Analysis
843 (PCA) Scatter plot of percentage data of calcareous nannofossil taxa of samples from the Cicogna
844 section in terms of the first and second component. Each sample is represented by a circle and
845 labelled. Green and blue shaded areas are the ellipses containing 95% of the data points of
846 Paleocene Group and Eocene group, respectively; B) Multivariate ANalysis Of VAriance (MANOVA).
847 Scatter graph and biplot. Each sample is represented by a black symbol (quadrangle and diamond)
848 and labelled. Green, red and blue shaded areas are the ellipses containing 95% of the data points of
849 Paleocene Group, PETM group and Eocene group, respectively.
850
851 **Figure 11.** Comparison of $\delta^{13}C$ profiles and semi-quantitative abundance patterns of selected
852 calcareous nannofossil taxa from the Cicogna section and ODP Site 1262. Calcareous nannofossil
853 biohorizons from DSDP Site 577 are reported in the right part of the figure. Orange and yellow bands
854 mark CIEs shown in previous figures. ). Color bands and symbols are the same as in previous figures.
855
856 **Plate I**. Images of selected calcareous nannofossil taxa from samples of the Cicogna section. Scale
857 bar 10μm.

**1.** *Discoaster lodoensis* Bramlette and Riedel, 1954. Parallel light. Parallel nicols. Sample CIC/07-492. **2-3.** *Girgisia gammation* (Bramlette Sullivan, 1961) Varol 1989. Crossed nicols. Sample CIC/07-437. **4-5.** *Chiphragmalithus calathus* Bramlette and Sullivan, 1961; 4.Parallel light; 5. Crossed nicols. Sample CIC/07-447. **6-7.** *Sphenolithus radians* Deflandre in Grassé, 1952. 6. Crossed nicols 0°; 7. Crossed nicols 45°. Sample CIC/07-437. **8.** *Tribrachiatus orthostylus* Shamrai, 1963. Parallel light. Sample 208-1262A-11H- 1, 149. Sample CIC/07-447. **9-10.** *Tribrachiatus contortus* (Stradner 1958) Bukry 1972. Parallel light. Sample CIC/07-335. **11-13.** *Zyghrablithus bijugatus* (Deflandre in Deflandre and Fert, 1954) Deflandre, 1959. Crossed nicols. Sample CIC/07-437. **14.** *Discoaster salisburgensis* Stradner, 1961. Parallel light. Sample CIC/07-335. **15.** *Discoaster diastypus* Bramlette and Sullivan, 1961. Parallel light. Sample CIC/07-335. **16.** *Fasciculithus tympaniformis* Hay and Mohler in Hay et al. 1967. Crossed nicols. Sample CIC/07-335. **17.** *Octolithus multiplus* (Perch-Nielsen, 1973) Romein, 1979. Crossed nicols. Sample CIC/07-122. **18.** *Discoaster multiradiatus* Bramlette and Riedel 1954. Parallel light. Sample CIC/07-122. **19.** *Toweius pertusus* (Sullivan, 1965) Romein, 1979. Crossed nicols. Sample CIC/07-122. **20.** *Toweius occultatus* (Locker, 1967) Perch-Nielsen, 1971. Crossed nicols. Sample CIC/07-122. **21.** *Toweius eminens* (Bramlette and Sullivan, 1961) Perch-Nielsen, 1971. Crossed nicols. Sample CIC/07-029. **22.** *Toweius eminens* (Bramlette and Sullivan, 1961) Perch-Nielsen, 1971. Crossed nicols. Sample CIC/07-029. **23.** *Toweius eminens* (Bramlette and Sullivan, 1961) Perch-Nielsen, 1971. Crossed nicols. Sample CIC/07-122. **24.** *Prinsius bisulcus* (Stradner, 1963) Hay and Mohler, 1967. Crossed nicols. Sample CIC/07-029. **25.** *Ericsonia robusta* Bramlette and Sullivan 1961. Crossed nicols. Sample CIC/07-029. **26-27.** *Sphenolithus anarrhopus* Bukry and Bramlette, 1969. 24. Crossed nicols 0°; 25. Crossed nicols 45°. Sample CIC/07-029. **28-29.** *Zyghrablithus bijugatus* (Deflandre in Deflandre and Fert, 1954) Deflandre, 1959. Crossed nicols. Sample CIC/07-122. **30.** *Thoracosphaera saxea* (Stradner, 1961). Crossed nicols. Sample CIC/07-122.

882

883 **Table 1**. Stratigraphic heights and ages of polarity chron boundaries, key calcareous nannofossil
884 datums, and CIEs at the Cicogna Section and ODP Site 1262.

885

886 **9. SUPPLEMENTARY INFORMATION**

887 **S1. Additional information on statistical analysis**

888 Nannofossil data from the Cicogna section (NE Italy) were subjected to statistical analysis using the
889 program PAST.

890 For PCA analysis, we additionally provide the biplot and the loading graphs of Component 1 and
891 Component 2 (**Figure S1**).

892 For non-metric multidimensional scaling (MDS) analysis, the species counts were combined to
893 produce a matrix of 15 genera. A square root transformation, used to standardize the matrix, was
894 chosen to minimize the influence of dominant taxa on the ordination (Schneider et al., 2011). Non-
895 metric multidimensional scaling (MDS), using the Bray–Curtis distance metric (**Figure S2**) was
896 applied in order to avoid assumptions as much as possible and guarantee the preservation of the
897 relative differences between the samples (McCune and Grace, 2002).

898 **References**

899 Schneider L.J., Bralower, T.J., Kump, L.R.: Response of nannoplankton to early Eocene ocean
900 destratification, Palaeogeogr., Palaeoclimatol., Palaeoecol., 310, 152-162, 2011.
901 McCune, B., Grace, J.B.: Analysis of Ecology Communities. MjM Software Design, Gleneden Beach,
902 Oregon, 2002.

903

904 **S2. Further explanation regarding biostratigraphic calcareous nannofossil counts**

905 The high abundance, widespread distribution and rapid evolution of calcareous nannofossils make
906 them one of the most powerful tool to date Cenozoic marine sediments. The use of semi-
907 quantitative counting and the gathering of high resolved datasets greatly enhance their correlation
908 potential (Backman et al., 2012; Agnini et al., 2014).

The methodology used in this study for samples of ODP Site 1262 is that proposed by Backman and Shackleton (1983), which consists in counting the number of calcareous nannofossils belonging to a specific taxon present in a prefixed area (1 $mm^2$). Because of significant dilution by terrigenous material in samples from the Cicogna section, we extended the study area to 9 $mm^2$. To further appreciate the importance of semi-quantitative estimates and high-resolution sampling, we compare the Top *D. multiradiatus* and Base *D. lodoensis* as recorded from the Cicogna section, ODP Site 1262 and DSDP Site 550 (**FigureS3**). At Cicogna and ODP Site 1262, we provide detailed abundance patterns of these two taxa. *Discoaster multiradiatus* shows a first decrease in abundance preceding the H1 event and a definitive disappearance just before the onset of the I1 event. *Discoaster lodoensis* displays a first presence in the I1 event, which is followed by an interval of absence that eventually leads to its continuous and common presence close to the onset of the X event (**Figure S3**). Datasets from the Cicogna section and ODP Site 1262 allow a very detailed characterization of these two biohorizons and the recognition of peculiar features that are not present in the low-resolution qualitative biostratigraphic data available for DSDP Site 550. As a consequence, the stratigraphic position of Top *D. multiradiatus* and Base *D. lodoensis* at DSDP Site 550 are inaccurate. We hope that this simple exercise could serve to emphasize the crucial importance of producing high-resolution semi-quantitative data to obtain the most reliable biostratigraphic results.

**References**

Ali, J. and Hailwood, E.: Magnetostratigraphic (re)calibration of the Paleocene/Eocene boundary interval in Holes 550 and 549, Goban Spur, eastern North Atlantic, Earth Planet. Sci. Lett., 161, 201-213, 1998.

Agnini, C., Fornaciari, E., Raffi, I., Rio, D., Röhl, U., and Westerhold, T.: High-resolution nannofossil biochronology of middle Paleocene to early Eocene at ODP Site 1262: implications for calcareous nannoplankton evolution. Mar. Micropaleontol., 64, 215-248, doi:10.1016/j.marmicro.2007.05.003, 2007b.

936 Agnini, C., Fornaciari, E., Raffi, I., Catanzariti, R., Pälike, H., Backman, J., and Rio, D.: Biozonation and
937 biochronology of Paleogene calcareous nannofossils from low and middle latitudes, Newslett.
938 Stratigr., 47, 131-181, doi:10.1127/0078-0421/2014/0042, 2014.
939 Backman, J., Raffi, I., Rio, D., Fornaciari, E. and Pälike, H., 2012: Biozonation and biochronology of
940 Miocene through Pleistocene calcareous nannofossils from low and middle latitudes, Newsl.
941 Stratigr., 45, 221-244.
942 Cramer, B. S., Wright, J. D., Kent, D. V., and Aubry, M.-P.: Orbital climate forcing of $\delta^{13}C$ excursions
943 in the late Paleocene–early Eocene (Chrons C24n–C25n), Paleoceanography, 18 (4), 1097,
944 doi:10.1029/2003PA000909, 2003.
945 Dallanave, E., Agnini, C., Muttoni, G., and Rio, D.: Magneto-biostratigraphy of the Cicogna section
946 (Italy): implications for the late Paleocene-early Eocene time scale, Earth Planet. Sci. Lett., 285,
947 39-51, doi:10.1016/j.epsl.2009.05.033, 2009.
948 Müller, C.: Biostratigraphic and paleoenvironmental interpretation of the Goban Spur region based
949 on a study of calcareous nannoplankton, Deep Sea Drill. Project, Initial Rep., 80, 389-414,
950 1985.
951 Westerhold, T., Röhl, U., Raffi, I., Fornaciari, E., Monechi, S., Reale, V., Bowles, J., and Evans, H. F.:
952 Astronomical calibration of the Paleocene time, Palaeogeogr. Palaeoclimatol. Palaeoecol.,
953 257, 377-403, doi:10.1016/j.palaeo.2007.09.016, 2008.
954 Zachos, J. C., Kroon, D., Blum, P., et al.: Early Cenozoic Extreme Climates: The Walvis Ridge Transect,
955 Proc. Ocean Drill. Program, Initial Rep., 208 doi:10.2973/odp.proc.ir.208.2004, 2004.
956
957 **S3. Looking through "frosty glass": Comparison to records at ODP Site 690**

958 We have presented fairly detailed records of bulk carbonate $\delta^{13}C$ and quantified calcareous
959 nannofossil assemblages for the lower Paleogene section at Cicogna, and compared these records
960 with those at the only two locations with similar information. From this comparison, we suggest
961 that a very detailed template exists for the alignment of $\delta^{13}C$ records and calcareous nannofossil
962 assemblage counts across the early Paleogene **(Figure 11**), one with much higher resolution than
963 given in most previous work, and one most likely related to changes in past global carbon cycling,
964 oceanography, and calcareous nannoplankton evolution.

965 Significant variations in calcareous nannofossil abundances definitely happened at multiple
966 locations during the PETM (Bralower, 2002, and references noted in main text). However, it is by no
967 means clear whether such changes extended across the broader early Paleogene, nor how such
968 changes might compare to those across the PETM. One can certainly speculate that variations in
969 calcareous nannofossil abundance records and bulk carbonate $\delta^{13}C$ records might correlate in fine
970 temporal detail across widely distributed sites throughout the early Paleogene, given well-

971 established calcareous nannofossil biozone schemes (Martini, 1971; Okada and Bukry, 1980; Agnini
972 et al., 2014), and a growing appreciation of a very dynamic carbon cycle over this time interval.
973 Nonetheless, the generation of detailed and coupled multi-million year records for quantified
974 calcareous nannofossil abundances and bulk carbonate $\delta^{13}C$ perplexed one of the referees for this
975 paper, who insisted that we needed to make comparisons with existing work at ODP Site 690 and
976 to explain discrepancies.

977 The lower Paleogene record at Site 690 provides a very good example in which to highlight the
978 basic background and importance of our work. Three holes were drilled and cored at ODP Site 690
979 on Maud Rise (South Atlantic; Figure 1) in 1987 using the advanced piston corer (APC) (Barker et al.,
980 1988). Sediment recovery within each core was nearly 100 %, although some cores were shorter
981 than the full 9.7 m. However, most of the lower Paleogene sequence was retrieved in only one of
982 the holes, 690B (Barker et al., 1988). This is important, because m-scale gaps generally occur
983 between successive cores during APC operations (Ruddiman et al., 1987; Lisiecki and Herbert, 2007).
984 The early Paleogene section at Site 690 is, almost assuredly, incomplete, with “missing” portions at
985 each core break.

986 Sediment from Core 690B-19H has been the focus of numerous papers, as it contains the PETM
987 (Kennett and Stott, 1991; Bains et al., 1999; Bralower, 2002). However, correlating this core to the
988 surrounding sedimentary record at Site 690, and the latter to early Paleogene records at other
989 locations is problematic, at least with any detail. For example, using Hole 690B records, Cramer et
990 al. (2003) estimated that 1.4 Myr occurred between the PETM and the H-1 event. This is incorrect,
991 as the duration is close to 1.8 Myr (Westerhold et al., 2008). Beyond the aforementioned core gaps,
992 there are major issues with the paleomagnetic record of early Paleogene sediments in Hole 690B
993 (Ali et al., 2000). Indeed, Ali et al. (2000) recommend using calcareous nannofossil records for
994 correlation purposes of this interval.

Records of bulk carbonate $\delta^{13}C$ (Cramer et al., 2003) and calcareous nannofossil relative abundances (Pospichal and Wise, 1990) have been generated using sediment at Hole 690B. When coupled together (**Figure S4**), these records show similarities to those at Cicogna (**Figure 11**). There is the long-term late Paleocene-early Eocene drop in $\delta^{13}C$ and several superimposed short-term negative CIEs. There are also closely coeval changes in calcareous nannofossil abundances, such as the peak in *D. multiradiatus* across the C event, the subsequent peak in *Fasciculithus* spp., and the cross-over of *T. contortus* and *T. orthostylus* just before the H-1 event. One can also see the problem with examining nannofossils at low depth/time resolution and qualitatively. We suggest here a "frosty glass" hypothesis, where details of Earth system change in the distant past are blurred presently by poorly resolved stratigraphy. This includes basic problems with aligning sections in depth and time, as well as interpretable quantification of data at high spatial resolution. Despite the need for additional work at Site 690, we suggest that available records at this location support the template offered in the main text.

**References**


Agnini, C., Fornaciari, E., Raffi, I., Catanzariti, R., Pälike, H., Backman, J., and Rio, D.: Biozonation and biochronology of Paleogene calcareous nannofossils from low and middle latitudes, Newslett. Stratigr., 47, 131-181, doi:10.1127/0078-0421/2014/0042, 2014.

Ali, J. R., Kent, D. V., and Hailwood, E. A.: Magnetostratigraphic reinvestigation of the Palaeocene/Eocene boundary interval in Hole 690B, Maud Rise, Antarctica, Geophys. J. Int., 141 (3), 639-646, doi: 10.1046/j.1365-246X.2000.00109.x, 2000.

Bains, S., Corfield, R. M. and Norris R. D.: Mechanisms of climate warming at the end of the Paleocene, Science, 285, 724-727, 1999.

Barker, P.E, Kennett, J.P., et al.: Proc. ODP, Init. Repts., 113, 1-774, doi:10.2973/odp.proc.ir.113.1988, 1988.

Bralower, T. .J.: Evidence of surface water oligotrophy during the Paleocene–Eocene thermal maximum: nannofossil assemblage data from Ocean Drilling Program Site 690, Maud Rise, Weddell Sea, Paleoceanography, 17, 1029-1042, doi:10.1029/2001PA000662, 2002.

Cramer, B. S., Wright, J. D., Kent, D. V., and Aubry, M.-P.: Orbital climate forcing of $\delta^{13}C$ excursions in the late Paleocene-early Eocene (Chrons C24n–C25n), Paleoceanography, 18 (4), 1097, doi:10.1029/2003PA000909, 2003.

Kennett, J. P. and Stott, L. D.: Abrupt deep-sea warming, palaeoceanographic changes and benthic extinctions at the end of the Palaeocene, Nature 353, 225-229 doi:10.1038/353225a0, 1991.

Lisiecki, L. E., and Herbert, T. D.: Automated composite depth scale construction and estimates of sediment core extension, Paleoceanography, 22(4), PA4213, doi:10.1029/2006PA001401, 2007.

Martini, E.: Standard Tertiary and Quaternary calcareous nannoplankton zonation, in: Proceedings of the 2nd Planktonic Conference, 2, Tecnoscienza, Roma, 739-785, 1971.
Okada, H., and Bukry, D.: Supplementary modification and introduction of code numbers to the low-latitude coccolith biostratigraphic zonation (Bukry, 1973; 1975), Mar. Micropaleontol., 5, 321-325, doi:10.1016/0377-8398(80)90016-X, 1980.
Pospichal, J. J., and Wise Jr., S. W.: Paleocene to middle Eocene calcareous nannofossils of Maud Rise, Weddell Sea, Proc. Ocean Drill. Program, Sci. Results, 113, 613-638, doi:10.2973/odp.proc.sr.113.205.1990, 1990.
Ruddiman, W. F., Cameron, D., and Clement, B. M.: Sediment disturbance and correlation of offset holes drilled with the hydraulic piston corer, Proc. Deep Sea Drill. Project, Init. Repts., 94, 615–634. doi:10.2973/dsdp.proc.94.111.1987, 1987.
Westerhold, T., Röhl, U., Raffi, I., Fornaciari, E., Monechi, S., Reale, V., Bowles, J., and Evans, H. F.: Astronomical calibration of the Paleocene time, Palaeogeogr. Palaeoclimatol. Palaeoecol., 257, 377-403, doi:10.1016/j.palaeo.2007.09.016, 2008.

**Supplementary figure captionsFigure S1**. PCA plots of calcareous nannofossil data from the Cicogna section (Italy). A) Loading plot of Component 1; B) Loading plot of Component 2; C) Biplot.

**Figure S2**. Non-metric multidimensional scaling (NMS) plot of calcareous nannofossil data from the Cicogna section (Italy). Grey dots = barren to virtually barren samples.

**Figure S3**. Abundance patterns of *D. multiradiatus* and *D. lodoensis* from the Cicogna section, ODP Site 1262 and DSDP Site 550. For these three successions paleomagnetic (Ali and Hailwood, 1998; Dallanave et al., 2009; Westerhold et al., 2008), carbon isotope (Cramer et al., 2003; Zachos et al., 2004; this study) and calcareous nannofossil data (Müller, 1985; Agnini et al., 2007, this study) are available. Top *D. multiradiatus* and Base *D. lodoensis* are clearly recognizable at Cicogna and ODP Site 1262, where quantitative counts have been performed. By contrast, qualitative data from DSDP Site 550 do not provide reliable biostratigraphic data P= present; R=rare; F=few; C=common; A=abundant; V=very abundant.

**Figure S4**. Carbon isotope data from ODP Site 690 (Cramer et al., 2003) plotted against qualitative abundance estimates of selected calcareous nannofossil taxa (Pospichal and Wei, 1990). Top *Fasciculithus* spp. (Aubry et al., 1996)

**Table S1**. Bulk carbonate stable isotopes and carbonate content of samples from the Cicogna section.

**Table S2**. Calcareous nannofossil assemblage counts for samples from the Cicogna section.

**Table S3.** Dataset used to perform the principal component analysis for calcareous nannofossil assemblages from the Cicogna section. Calcareous nannofossils are subdivided in 15 subgroups (*Chiasmolithus, Coccolithus, Ellipsolithus, Discoaster, Ericsonia, Fascicuithus, Girgisia, Octolithus, Prinsius, Sphenolithus, Toweius, Rhomboaster/Tribrachiatus, Zyghrablithus*, reworking, others). In order to avoid the closed-sum effect that derives from the use of percentage data, we apply a log transformation of raw data.

**Table S4.** Dataset used to perform the non-metric multidimensional scaling (MDS) for calcareous nannofossil assemblages from the Cicogna section. Calcareous nannofossils are subdivided in 15 subgroups (*Chiasmolithus, Coccolithus, Ellipsolithus, Discoaster, Ericsonia, Fascicuithus, Girgisia, Octolithus, Prinsius, Sphenolithus, Toweius, Rhomboaster/Tribrachiatus, Zyghrablithus*, reworking, others). A square root transformation was used to minimize the influence of dominant taxa on the ordination.

## 10 REFERENCES


Adelseck Jr., C. G., Geehan, G. W., and Roth, P. H.: Experimental evidence for the selective dissolution and overgrowth of calcareous nannofossils during diagenesis, Geol. Soc. Am. Bull., 84, 2755-2762, 1973.

Agnini, C., Muttoni, G., Kent, D. V., and Rio, D.: Eocene biostratigraphy and magnetic stratigraphy from Possagno, Italy: The calcareous nannofossil response to climate variability, Earth Planet. Sci. Lett., 241, 815-830, doi:10.1016/j.epsl.2005.11.005, 2006.

Agnini, C., Fornaciari, E., Rio, D., Tateo, F., Backman, J., and Giusberti, L.: Responses of calcareous nannofossil assemblages, mineralogy and geochemistry to the environmental perturbations across the Paleocene/Eocene boundary in the Venetian Pre–Alps, Mar. Micropaleontol., 63, 19-38, doi:10.1016/j.marmicro.2006.10.002, 2007a.

Agnini, C., Fornaciari, E., Raffi, I., Rio, D., Röhl, U., and Westerhold, T.: High-resolution nannofossil biochronology of middle Paleocene to early Eocene at ODP Site 1262: implications for calcareous nannoplankton evolution. Mar. Micropaleontol., 64, 215-248, doi:10.1016/j.marmicro.2007.05.003, 2007b.

Agnini, C., Macrì, P., Backman, J., Brinkhuis, H., Fornaciari, E., Giusberti, L., Luciani, V., Rio, D., Sluijs, A., and Speranza, F.: An early Eocene carbon cycle perturbation at 52.5 Ma in the Southern Alps: Chronology and biotic response, Paleoceanography, 24, PA2209, doi:10.1029/2008PA001649, 2009.

Agnini, C., Fornaciari, E., Giusberti, L., Grandesso, P., Lanci, L., Luciani, V., Muttoni, G., Pälike, H., Rio, D., Spofforth, D. J. A., and Stefani, C.: Integrated bio-magnetostratigraphy of the Alano section (NE Italy): a proposal for defining the middle-late Eocene boundary, Geol. Soc. Am. Bull., 123, 841-872, doi:10.1130/B30158.1, 2011.

Agnini, C., Fornaciari, E., Raffi, I., Catanzariti, R., Pälike, H., Backman, J., and Rio, D.: Biozonation and biochronology of Paleogene calcareous nannofossils from low and middle latitudes, Newslett. Stratigr., 47, 131-181, doi:10.1127/0078-0421/2014/0042, 2014.

Aitchison, J.: The Statistical Analysis of Compositional Data. Chapman and Hall, London - New York, 12, 1-416, 1986.

Alcober, J. A. and Jordan, R. W.: An interesting association between *Neosphaera coccolithomorpha* and *Ceratolithus cristatus,* Eur. J . Phycol, 32, 91-93, 1997.

Angori, E., Bernaola, G., and Monechi, S.: Calcareous nannofossil assemblages and their response to the Paleocene-Eocene Thermal Maximum event at different latitudes: ODP Site 690 and Tethyan sections, Geol. Soc. Am. Spec. Pap., 424, 69-85, doi:10.1130/2007.2424(04), 2007.

Aubry, M.-P.: Handbook of Cenozoic Calcareous Nannoplankton, book 1, Ortholithae (Discoaster), Am. Mus. Nat. Hist. Micropaleontol. Press, New York, 1-263, 1984.

Aubry, M.-P.: Handbook of Cenozoic Calcareous Nannoplankton, book 2, Ortholithae (Holococcoliths, Ceratoliths, Ortholiths and Other), Am. Mus. Nat. Hist. Micropaleontol. Press, New York, 1-279, 1988.

Aubry, M.-P.: Handbook of Cenozoic Calcareous Nannoplankton, book 3, Ortholithae (Pentaliths and Other), Heliolithae (Fasciculiths, Sphenoliths and Other), Am. Mus. Nat. Hist. Micropaleontol. Press, New York, 1-279, 1989.

Aubry, M.-P.: Handbook of Cenozoic Calcareous Nannoplankton, book 4, Heliolithae (Helicoliths, Cribriliths, Lopadoliths and Other), Am. Mus. Nat. Hist. Micropaleontol. Press, New York, 1-381, 1990.

Aubry, M.-P.: Early Paleogene calcareous nannoplankton evolution: a tale of climatic amelioration, in: Late Paleocene–early Eocene Biotic and Climatic Events in the Marine and Terrestrial Records, Columbia University Press, New York, 158-201, 1998.

Aubry, M.-P.: Handbook of Cenozoic Calcareous Nannoplankton, book 5, Heliolithae (Zygoliths and Rhabdoliths), Am. Mus. Nat. Hist. Micropaleontol. Press, New York, 1-368, 1999.

Aubry, M.-P.: Late Paleocene–early Eocene sedimentary history in western Cuba: implications for the LPTM and for regional tectonic history, Micropaleontol., 45, 5-18, 1999.

Aubry, M.-P. and Salem, R.: The Dababiya Core: A window into Paleocene to early Eocene depositional history in Egypt based on coccolith stratigraphy, Stratigraphy, 9, 287-346, 2012.

Baccelle, L. and Bosellini, A.: Diagrammi per la stima visiva della composizione percentuale nelle rocce sedimentary, Ann. Univ. Ferrara, 9, 4, 59-62, 1965.

Backman, J.: Late Paleocene to middle Eocene calcareous nannofossil biochronology from the Shatsky Rise, Walvis Ridge and Italy, Palaeogeogr. Palaeoclimatol. Palaeoecol., 57, 43-59, 1986.

Backman, J. and Shackleton N. J.: Quantitative biochronology of Pliocene and early Pleistocene calcareous nannoplankton from the Atlantic, Indian and Pacific Oceans, Mar. Micropaleontol., 8, 141-170, doi:10.1016/0377-8398(83)90009-9, 1983.

Baumann, K.-H., Andruleit, H., Böckel, B., Geisen, M., and Kinkel, H.: The significance of extant coccolithophores as indicators of ocean water masses, surface water temperature, and palaeoproductivity: a review, Paläontol. Zeitsch., 79, 93-112, 2005.

Bernoulli, D., and Jenkyns, H.C.: Alpine, Mediterranean, and Central Atlantic Mesozoic facies in relation to the early evolution of the Tethys, in: Modern and Ancient Geosynclinal Sedimentation, Society for Sedimentary Geology (SEPM) Special Publication, 19, 19–160, 1974.

Bernoulli, D., Caron, C., Homewood, P., Kalin, O., and Van Stuijvenberg, J.: Evolution of continental margins in the Alps, Schweiz. Miner. Petrog., 59, 165-170, 1979.

Bijl, P. K., Schouten, S., Sluijs, A., Reichart, G. J., Zachos, J. C., Brinkhuis, H.: Early Palaeogene temperature evolution of the southwest Pacific Ocean, Nature, 461, 776–779, doi:10.1038/nature08399, 2009.

Billard, C. and Innouye, I.: What is new in coccolithophore biology?, in: Coccolithophores - From Molecular Processes to Global Impact, Springer, Berlin, 1-29, 2004.

Bordiga, M., Henderiks, J., Tori, F., Monechi, S., Fenero, R., and Thomas, E.: The Eocene–Oligocene transition at ODP Site 1263, Atlantic Ocean: decreases in nannoplankton size and abundance and correlation with benthic foraminiferal assemblages, Clim. Past Discuss., 11, 1615-1664, doi:10.5194/cpd-11-1615-2015, 2015.

Bornemann, A. and Mutterlose, J.: Calcareous nannofossil and $\delta^{13}C$ records from the Early Cretaceous of the Western Atlantic Ocean: evidence for enhanced fertilization across the Berriasian–Valanginian transition, Palaios, 23, 821-832, 2008.

Boucot, A. J.: Evolution and Extinction Rate Controls. Elsevier, Amsterdam, The Netherlands, 250p. 1975.

Bown, P. R.: Paleogene calcareous nannofossils from the Kilwa and Lindi areas of coastal Tanzania: Tanzania Drilling Project Sites 1 to 10, J. Nannoplankt. Res., 27, 21-95, 2005.

Bown, P., and Pearson, P.: Calcareous plankton evolution and the Paleocene/Eocene thermal maximum event: New evidence from Tanzania, Mar. Micropaleontol., 71, 60-70, doi: 10.1016/j.marmicro.2009.01.005, 2009.

Bown, P. R. and Young, J. R.: Techniques, in: Calcareous Nannofossil Biostratigraphy, Chapman & Hall, London, 16-28, 1998.

Bown, P. R., Lees, J. A., and Young, J. R.: Calcareous nannoplankton evolution and diversity through time, in: Coccolithophores - From Molecular Processes to Global Impact, Springer, Berlin, 481-508, 2004.

Bralower, T..J.: Evidence of surface water oligotrophy during the Paleocene–Eocene thermal maximum: nannofossil assemblage data from Ocean Drilling Program Site 690, Maud Rise, Weddell Sea, Paleoceanography, 17, 1029-1042, doi:10.1029/2001PA000662, 2002.

Bralower,T. J., Mutterlose, J.: Calcareous nannofossil biostratigraphy of ODP Site 865, Allison Guyot, Central Pacific Ocean: a tropical Paleogene reference section. Proc Ocean Drill Prog Sci Results, 143, 31-72, doi:10.2973/odp.proc.sr.143.204.1995, 1995.

Broecker, W. S. and Peng, T.-H.: Tracers in the Sea, Eldigio Press, LamontDoherty Geological Observatory, Palisades, New York, 1-690, 1982.

Buccianti, A., Mateu-Figueras, G., Pawlowsky-Glahn, V.: Compositional data analysis in the geosciences: From theory to practice, Geol. Soc. London, London, Spec. Publ., 264, 1- 12, doi: 10.1144/GSL.SP.2006.264, 2006.Bukry, D.: Low-latitude coccolith biostratigraphic zonation. Initial Rep. Deep Sea Drill. Proj., 15, 685–703, 1973.

Cati, A., Sartorio, D., and Venturini, S.: Carbonate platforms in the subsurface of the northern Adriatic area, Mem. Soc. Geol. It., 40, 295-308, 1989.

Corfield, R. M.: Palaeocene oceans and climate: An isotopic perspective, Earth Sci. Rev., 37, 225-252, doi.org/10.1016/0012-8252(94)90030-2, 1994.

Costa, V., Doglioni, C., Grandesso, P., Masetti, D., Pellegrini, G.B., and Tracanella, E.: Carta Geologica d'Italia, Foglio 063, Belluno: Roma, Servizio Geologico d'Italia, scale 1:50,000, 1 sheet + 74 p., 1996.

Cramer, B. S., Wright, J. D., Kent, D. V., and Aubry, M.-P.: Orbital climate forcing of $\delta^{13}C$ excursions in the late Paleocene– early Eocene (Chrons C24n –C25n), Paleoceanography, 18 (4), 1097, doi:10.1029/2003PA000909, 2003.

Cramer, B. S., Toggweiler, J. R., Wright, J. D., Katz, M. E., and Miller, K. G.: Ocean overturning since the Late Cretaceous: Inferences from a new benthic foraminiferal isotope compilation, Paleoceanogaphy, 24, PA4216, doi:10.1029/2008PA001683, 2009.

Dallanave, E., Agnini, C., Muttoni, G., and Rio, D.: Magneto-biostratigraphy of the Cicogna section (Italy): implications for the late Paleocene-early Eocene time scale, Earth Planet. Sci. Lett., 285, 39-51, doi:10.1016/j.epsl.2009.05.033, 2009.

Dallanave, E., Agnini, C., Bachtadse, V., Muttoni, G., Crampton, J. S., Strong, C. P., Hines, B. R., Hollis, C. J., and Slotnick., B. S.: Early to middle Eocene magnetostratigraphy of the southwest Pacific Ocean and climate influence on sedimentation: insights from the Mead Stream section, New Zealand, Geol. Soc. Am. Bull., 127, 643-660, doi: 10.1130/B31147.1, 2015.

DeConto, R. M., Galeotti, S., Pagani, M., Tracy, D., Schaefer, K. Zhang, T., Pollard, D., and Beerling D. J.: Past extreme warming events linked to massive carbon release from thawing permafrost, Nature, 484, 87-91, doi:10.1038/nature10929, 2012.

Dickens, G. R.: Methane oxidation during the late Palaeocene thermal maximum, Bull. Soc. Geol. France, 171 (1), 37-49, 2000.

Dickens, G. R.: Rethinking the global carbon cycle with a large, dynamic and microbially mediated gas hydrate capacitor, Earth Planet. Sci. Lett., 213, 169-183, 2003.

Dickens, G. R. and Backman, J.: Core alignment and composite depth scale for the lower Paleogene through uppermost Cretaceous interval at Deep Sea Drilling Project Site 577, Newslett. Stratigr., 46, 47-68, doi:10.1127/0078-0421/2013/0027, 2013.

Dickens, G. R., Castillo, M. M., and Walker, J. C. G.: A blast of gas in the latest Paleocene: Simulating first-order effects of massive dissociation of oceanic methane hydrate, Geology, 25, 259–262, 1997.

Doglioni, C. and Bosellini, A.: Eoalpine and mesoalpine tectonics in the Southern Alps, Geol. Rundsch., 77, 734-754, 1987.

Dupuis, C., Aubry, M.-P., Steurbaut, E., Berggren, W.A., Ouda, K., Magioncalda, R., Cramer, B.S., Kent, D.V., Speijer, R.P., and Heilmann-Clausen, C.: The Dababiya Quarry section: lithostratigraphy, geochemistry and paleontology. Micropaleontology, 49 (suppl. 1), 41–59. 2003.

Erba, E., Bottini, C., Weissert, H. J., Keller, C. E.: Calcareous nannoplankton response to surface-water acidification around Oceanic Anoxic Event 1a. Science 329, 428, doi: 10.1126/science.1188886, 2010.

Frank, T. D., Arthur, M. A., and Dean W. E.: Diagenesis of Lower Cretaceous pelagic carbonates, North Atlantic: paleoceanographic signals obscured, J. Foraminiferal Res., 29, 340–351, 1999.

Galeotti, S., Krishnan, S., Pagani, M., Lanci, L., Gaudio, A., Zachos, J. C., Monechi, S., Morelli, G., and Lourens, L.: Orbital chronology of early Eocene hyperthermals from the Contessa Road section, central Italy, Earth Planet. Sci. Lett., 290, 192-200, doi:10.1016/j.epsl.2009.12.021, 2010.

Geisen, M., Young, J. R., Probert, I., Sáez, A. G., Baumann, K.-H., Bollmann, J., Cros, L., De Vargas, C., Medlin, L. K., and Sprengel, C.: Species level variation in coccolithophores, in: Coccolithophores –From Molecular Processes to Global Impact, Springer, Berlin, 327-366, 2004.

Gibbs, S. J., Shackleton, N. J., and Young, J. R.: Orbitally forced climate signals in mid-Pliocene nannofossil assemblages, Mar. Micropaleontol., 51, 39-56, 2004.

Gibbs, S. J., Bown, P. R., Sessa, J. A., Bralower, T. J., and Wilson, P. A.: Nannoplankton extinction and origination across the Paleocene-Eocene thermal maximum, Science, 314, 1770-1773, doi:10.1126/science.1133902, 2006a.

Gibbs, S. J., Bralower, T .J., Bown, P. R., Zachos, J. C., and Bybell, L.M.: Shelf and open-ocean calcareous phytoplankton assemblages across the Paleocene–Eocene thermal maximum: implications for global productivity gradients, Geology, 34, 233-236, doi:10.1130/G22381.1, 2006b.

Gibbs, S. J., Bown, P. R., Murphy, B. H., Sluijs, A., Edgar, K. M., Pälike, H., Bolton, C. T., and Zachos, J.C.: Scaled biotic disruption during early Eocene global warming events, Biogeosciences, 9, 4679-4688, doi:10.5194/bg-9-4679-2012, 2012.

Giusberti, L., Rio, D., Agnini, C., Backman, J., Fornaciari, E., Tateo, F., and Oddone, M.: Mode and tempo of the Paleocene-Eocene Thermal Maximum in an expanded section in the Venetian Pre-Alps, Geol. Soc. Am. Bull., 119, 391-412, doi:10.1130/B25994.1, 2007.

Giusberti, L., Boscolo Galazzo, F., and Thomas, E.: Benthic foraminifera at the Paleocene/Eocene thermal maximum in the western Tethys (Forada section): variability in climate and productivity, Clim. Past Discuss., 11, 4205-4272, doi:10.5194/cpd-11-4205-2015, 2015.Grandesso, P.: Biostratigrafia delle formazioni terziarie del Vallone Bellunese, Boll. Soc. Geol. Ital., 94, 1323-1348, 1976.

Hallock, P.: Fluctuations in the trophic resource continuum: A factor in global diversity cycles?, Paleoceanography, 2, 457–471, 1987.

Hammer, Ø, Harper, D. A. T., and Ryan, P. D.: PAST: Paleontological statistics software package for education and data analysis, Palaeontol. Electron., 4, 9 pp., 2001.

Haq, B. U. and Lohmann, G. P.: Early Cenozoic calcareous nannoplankton biogeography of the Atlantic Ocean, Mar. Micropaleontol., 1, 119-194, 1976.

Harris, A.D., Miller, K.G., Browning, J. V., Sugarman, P.J., Olsson, R.K., Cramer, B.S. and Wright, J.D.;. Integrated stratigraphic studies of Paleocene- lowermost Eocene sequences, New Jersey

Coastal Plain: Evidence for glacioeustatic control. Paleoceanography, 25, PA3211, doi:10.1029/2009PA001800, 2010.Hay, W. W.: Carbonate fluxes and calcareous nannoplankton, in: Coccolithophores - From Molecular Processes to Global Impact, Springer, Berlin, 508-528, 2004.

Hönisch, B., Ridgwell, A., Schmidt, D. N., Thomas, E., Gibbs, S.J., Sluijs, A., Zeebe, R., Kump, L., Martindale, R. C., Greene, S. E., Kiessling, W., Ries, J., Zachos, J. C., Royer, D. L., Barker, S., Marchitto Jr., T. M., Moyer, R., Pelejero, C., Ziveri, P., Foster, G. L., and Williams, B.: The geological record of ocean acidification, Science, 335, 1058-1063, doi:10.1126/science.1208277, 2012.

Hollis, C.J., Taylor, K. W. R., Handley, L., Pancost, R. D., Huber, M., Creech, J. B., Hines, B.R., Crouch, E. M., Morgans, H. E. G., Crampton, J. S., Gibbs, S., Pearson, P. N., and Zachos, J. C.: Early Paleogene temperature history of the southwest Pacific Ocean: Reconciling proxies and models, Earth Planet. Sci. Lett., 349-350, 53-66, 2012.

Huber, M., and Caballero, R.: The Early Eocene equable climate problem revisited, Clim. Past, 7, 603-633, 2011.

Iglesias-Rodriguez, M. D., Halloran, P. R., Rickaby, R. E. M., Hall, I. R., Colmenero-Hidalgo, E., Gittins, J. R., Green, D. R. H., Tyrrell, T., Gibbs, S. J., Von Dassow, P., Rehm, E., Armbrust, E. V., and Boessenkool, K. P.: Phytoplankton calcification in a high-$CO_2$ world, Science, 320, 336-340, doi:10.1126/science.1154122, 2008.

Jiang, S., and Wise Jr., S.W: Distinguishing the influence of diagenesis on the paleoecological reconstruction of nannoplankton across the Paleocene/Eocene Thermal Maximum: An example from the Kerguelen Plateau, southern Indian Ocean, Mar. Micropaleontol., 72, 49-59, doi: 10.1016/j.marmicro.2009.03.003, 2009.

Keeling, C. D. and Whorf, T. P.: Atmospheric carbon dioxide record from Mauna Loa, in: Oak Ridge Laboratory Trends: A Compendium of Data on Global Change. Carbon Dioxide Information Analysis Center, Oak Ridge National Laboratory, U.S. Department of Energy, Oak Ridge, Tennessee, U.S.A., http://cdiac.esd.ornl.gov/trends/co2/sio-keel-flask/sio-keel-flask.html, 2004.

Kirtland-Turner, S., Sexton, P. F., Charles, C. D., and Norris, R. D.: Persistence of carbon release events through the peak of early Eocene global warmth, Nature Geosci., 7, 748-751, doi:10.1038/ngeo2240, 2014.

Kleypas, J. A., Feely, R. A., Fabry, V. J., Langdon, C., Sabine, C. L., and Robbins, L. L.: Impacts of ocean acidification on coral reefs and other marine calcifiers: A guide for future research, Contrib. No. 2857, NOAA/Pacific Marine Environm. Lab., 88 pp., 2006.

Komar, N., Zeebe, R. E., and Dickens, G.R.: Understanding long-term carbon cycle trends: The late Paleocene through the early Eocene. Paleoceanography, 28, 650-662, doi:10.1002/palo.20060, 2013.

Krishnan, S., Pagani, M., Agnini, C.: Leaf waxes as recorders of paleoclimatic changes during the Paleocene-Eocene Thermal Maximum: Regional expressions from the Belluno Basin. Organic Geochemistry, 80, 8-17, doi: 10.1016/j.orggeochem.2014.12.005, 2015.

Kroopnick, P. M.: The distribution of $^{13}C$ of $\Sigma CO_2$ in the world oceans, Deep Sea Res. Part A, 32, 57-84, 1985.

Kucera, M., Malmgren, B.A.: Logratio transformation of compositional data — a resolution of the constant sum constraint, Mar. Micropaleontol., 34, 117-120, 1998.Kump, L. R., Bralower, T. J., and Ridgwell, A.: Ocean acidification in deep time, Oceanography, 22, 94-107, 2009.

Kurtz, A. C., Kump, L. R., Arthur, M. A., Zachos, J. C., and Paytan, A.: Early Cenozoic decoupling of the global carbon and sulfur cycles, Paleoceanography, 18, 1090, doi:10.1029/2003PA000908, 2003.

Langer, G., M., Geisen, Baumann, K.-H., Kläs, J., Riebesell, U., Thoms, S., and Young, J. R.: Species-specific response of calcifying algae to changing seawater carbonate chemistry, Geochem. Geophys. Geosyst., 7, Q09006, doi:10.1029/2005GC001227, 2006.

Leon-Rodriguez, L. and Dickens, G. R.: Constraints on ocean acidification associated with rapid and massive carbon injections: The early Paleogene record at Ocean Drilling Program Site 1215, Equatorial Pacific Ocean, Palaeogeogr. Palaeoclimatol. Palaeoecol., 298, 409-420, doi:org/10.1016/j.palaeo.2010.10.029, 2010.

Lohbeck, K. T., Riebesell, U., and Reusch, T. B. H.: Adaptive evolution of a key phytoplankton species to ocean acidification, Nature Geosci., 5, 346-351, doi:10.1038/ngeo1441, 2012.

Lourens, L. J., Sluijs, A., Kroon, D., Zachos, J. C., Thomas, E., Röhl, U., Bowles, J., and Raffi, I.: Astronomical pacing of late Palaeocene to early Eocene global warming events, Nature, 435, 1083-1087, doi:10.1038/nature03814, 2005.

Lunt, D. J., Ridgwell, A., Sluijs, A., Zachos, J. C., Hunter, S., and Haywood, A.: A model for orbital pacing of methane hydrate destabilization during the Palaeogene, Nature Geosci., 4, 775-778, doi:10.1038/ngeo1266, 2011.

MacArthur, R. and Wilson, E .O.: The Theory of Island Biogeography, Princeton University Press, ISBN 0-691-08836-5M, 1967.

Marino, M., Maiorano, P., and Lirer, F.: Changes in calcareous nannofossil assemblages during the Mid-Pleistocene Revolution, Mar. Micropaleontol., 69, 70-90, doi:10.1016/j.marmicro.2007.11.010, 2008.

Martini, E.: Standard Tertiary and Quaternary calcareous nannoplankton zonation, in: Proceedings of the 2nd Planktonic Conference, 2, Tecnoscienza, Roma, 739-785, 1971.

Matter, A., Douglas, R. G., and Perch-Nielsen, K: Fossil preservation, geochemistry and diagenesis of pelagic carbonates from Shatsky Rise, northwest Pacific, Init. Rep. DSDP, 32, 891–922, 1975.

Mixon, R.B. and Powars D.S.: Folds and faults in the inner Coastal Plain of Virginia and Maryland: their effect on the distribution and thickness of Tertiary rock units and local geomorphic history. In Frederiksen N.O., and Kraft K. (Eds.), Cretaceous and Tertiary Stratigraphy, paleontology, and structure, southwestern Maryland and northeastern Virginia. American Association of Stratigraphic Palynologists Field Trip Volume and Guidebook (1984), 112–122, 1994

Milliman, J. D.: Production and accumulation of calcium carbonate in the ocean: Budget of a nonsteady state. Global Biogeochemical Cycles, 7, 927-957, doi: 10.1029/93GB02524, 1993.

Monechi, S., Angori, E., von Salis, K.: Calcareous nannofossil turnover around the Paleocene/Eocene transition at Alamedilla (southern Spain). Bull. Soc. Geol. Fr., 171, 477–489, 2000.

Mutterlose, J., Linnert, C., and Norris, R.: Calcareous nannofossils from the Paleocene–Eocene Thermal Maximum of the equatorial Atlantic (ODP Site 1260B): Evidence for tropical warming, Mar. Micropaleontol., 65, 13-31, doi:10.1016/j.marmicro.2007.05.004, 2007.

Nicolo, M. J., Dickens, G. R., Hollis, C. J., and Zachos, J. C.: Multiple early Eocene hyperthermals: Their sedimentary expression on the New Zealand continental margin and in the deep sea, Geology, 35, 699-702, doi:10.1130/G23648A.1, 2007.

Norris, R.D., Wilson, P.A, Blum, P., and the Expedition 342 Scientists: Expedition 342 summary. Proc. IODP, 342, 1-149, doi:10.2204/iodp.proc.342.2014, 2014.

Ogg, J.G., and Bardot, L.: Aptian through Eocene magnetostratigraphic correlation of the Blake Nose Transect (Leg 171B), Florida continental margin, Proc. ODP, Sci. Results, 171B, 1-58, doi:10.2973/odp.proc.sr.171B.104.2001 2001.

Okada, H., and Bukry, D.: Supplementary modification and introduction of code numbers to the low-latitude coccolith biostratigraphic zonation (Bukry, 1973; 1975), Mar. Micropaleontol., 5, 321-325, doi:10.1016/0377-8398(80)90016-X, 1980.

Pälike, H., Lyle, M. W., Nishi, H., Raffi, I., Ridgwell, A., Gamage, K., Klaus, A., Acton, G. D., Anderson, L., Backman, J., Baldauf, J. G., Beltran, C., Bohaty, S. M., Bown, P. R., Busch, W. H., Channell, J. E. T., Chun, C. O. J., Delaney, M. L., Dewang, P., Dunkley Jones, T., Edgar, K. M., Evans, H. F., Fitch, P., Foster, G. L., Gussone, N., Hasegawa, H., Hathorne, E. C., Hayashi, H., Herrle, J. O., Holbourn, A. E. L., Hovan, S. A., Hyeong, K., Iijima, K., Ito, T., Kamikuri, S.-I., Kimoto, K., Kuroda, J., Leon-Rodriguez, L., Malinverno, A., Moore, T. C., Murphy, B., Murphy, D. P., Nakamura, H., Ogane, K., Ohneiser, C., Richter, C., Robinson, R. S., Rohling, E. J., Romero, O. E., Sawada, K., Scher, H. D., Schneider, L., Sluijs, A., Takata, H., Tian, J., Tsujimoto, A., Wade, B. S., Westerhold, T., Wilkens, R. H., Williams, T., Wilson, P. A., Yamamoto, Y., Yamamoto, S., Yamazaki, T., and Zeebe, R. E.: A Cenozoic record of the equatorial Pacific carbonate compensation depth, Nature, 488, 609-614, doi:10.1038/nature11360, 2012

Payros, A., Ortiz, S., Millán, I., Arostegi, J., Orue-Etxebarria, X., and Apellaniz, E.: Early Eocene climatic optimum: Environmental impact on the north Iberian continental margin, Geol. Soc. Am. Bull.,127, 1632-1644doi:10.1130/B31278.1, 2015.

Pearson, P. N., van Dongen, B. E., Nicholas, C. J., Pancost, R. D., Schouten, S., Singano, J. M., and Wade, B. S.: Stable warm tropical climate through the Eocene Epoch, Geology, 35, 211-214, 2007.

Perch-Nielsen, K.: Cenozoic calcareous nannofossils, in: Plankton stratigraphy, Cambridge Univ. Press, New York, 427-554, 1985.

Pianka, E. R.: On r and K selection. Amer. Natural., 104, 592-597, doi:10.1086/282697, 1970.

Premoli Silva, I. and Sliter, W.V.: Cretaceous paleoceanography: Evidence from planktonic foraminiferal evolution, Geol. Soc. Am. Spec. Pap., 332, 301-328, doi:10.1130/0-8137-2332-9.301, 1999.

Raffi, I., Backman, J., and Pälike, H.: Changes in calcareous nannofossil assemblage across the Paleocene/Eocene transition from the paleo-equatorial Pacific Ocean, Palaeogeogr. Palaeoclimatol. Palaeoecol., 226, 93-126, doi:10.1016/j.palaeo.2005.05.006, 2005.

Raffi, I., and De Bernardi, B.: Response of calcareous nannofossils to the Paleocene-Eocene Thermal Maximum: Observations on composition, preservation and calcification in sediments from ODP Site 1263 (Walvis Ridge - SW Atlantic), Mar. Micropaleontol., 69, 119-138, doi: 10.1016/j.marmicro.2008.07.002, 2008.

Raffi, I., Backman, J., Zachos, J.C., Sluijs, A.: The response of calcareous nannofossil assemblages to the Paleocene Eocene Thermal Maximum at the Walvis Ridge in the South Atlantic. Mar. Micropaleontol., 70, 201-212, doi:10.1016/j.marmicro.2008.12.005, 2009.

Riebesell, U., Zondervan, I., Rost, B., Tortell, P. D., Zeebe, R. E., and Morel, F. M. M.: Reduced calcification of marine plankton in response to increased atmospheric $CO_2$, Nature, 407, 364-367, doi:10.1038/35030078, 2000.

Riebesell, U., Bellerby, R. G. J., Engel, A., Fabry, V. J., Hutchins, D. A., Reusch, K.G., Schulz, T. B. H., and Morel, F. M. M.: Comment on "Phytoplankton calcification in a high-CO2 world", Science, 322, 1466b, doi:10.1126/science.1161096, 2008.

Romein, A.J.T.: Lineages in early Paleogene calcareous nannoplankton. Utrecht Micropaleont. Bull., 22, 1-231, 1979.

Rost, B. and Riebesell, U.: Coccolithophores and the biological pump: responses to environmental changes, in: Coccolithophores - From Molecular Processes to Global Impact, Springer, Berlin, 99-125, 2004.

Roth, P.H.: Jurassic and Lower Cretaceous calcareous nannofossils in the western North Atlantic (Site 534): biostratigraphy, preservation, and some observations on biogeography and paleoceanography, DSDP Init. Repts., 76, 587-621, 1983.

Roth, P.H., and Thierstein, H.R.: Calcareous nannoplankton: Leg XIV of the Deep Sea Drilling Project, DSDP Init. Repts., 14, 421-486, 1972.
Schrag, D.P., DePaolo, D.J., and Richter, F.M.: Reconstructing past sea surface temperatures: correcting for diagenesis of bulk marine carbonate, Geochim. Cosmochim. Acta, 59, 2265-2278, 1995.
Scholle P. A., and Arthur, M. A.: Carbon isotope fluctuations in Cretaceous pelagic limestones: potential stratigraphic and petroleum exploration tool, Amer. Assoc. Pet. Geol. Bulletin, 64, 67-87, 1980.
Self-Trail, J. M., Powars, D. S., Watkins, D. K., and Wandless, G.: Calcareous nannofossil assemblage changes across the Paleocene-Eocene thermal maximum: Evidence from a shelf setting, Mar. Micropaleontol., 92-93, doi:10.1016/j.marmicro.2012.05.003, 2012.
Shackleton, N. J.: Paleogene stable isotope events, Palaeogeogr. Palaeoclimatol. Palaeoecol., 57, 91-102, 1986.
Shamrock, J.L.: Eocene calcareous nannofossil biostratigraphy, paleoecology and biochronology of ODP Leg 122 Hole 762c, Eastern Indian Ocean (Exmouth Plateau). PhD thesis, University of Nebraska, 2010.
Slotnick, B. S., Dickens, G. R., Nicolo, M. J., Hollis, C. J., Crampton, J. S., Zachos, J. C., and Sluijs, A.: Large-amplitude variations in carbon cycling and terrestrial weathering during the latest Paleocene and earliest Eocene: The record at Mead Stream, New Zealand, J. Geol., 120, 1-19, doi:10.1086/666743, 2012.
Slotnick, B. S., Lauretano, V., Backman, J., Dickens, G. R., Sluijs, A., and Lourens, L.: Early Paleogene variations in the calcite compensation depth: new constraints using old borehole sediments from across Ninetyeast Ridge, central Indian Ocean, Clim. Past, 11, 473-493, , doi:10.5194/cp-11-473-2015, 2015a.
Slotnick, B. S., Dickens, G. R., Hollis, C. J., Crampton, J. S., Strong, C. P., and Phillips, A.: The onset of the Early Eocene Climatic Optimum at Branch Stream, Clarence River valley, New Zealand, New Zeal. J. Geol. Geophys., 58, 262-280 doi: 10.1080/00288306.2015.1063514, 2015b.
Spofforth, D. J. A., Agnini, C., Pälike, H., Rio, D., Fornaciari, E., Giusberti, L., Luciani, V., Lanci, L., Muttoni, G., and Bohaty, S. M.: Organic carbon burial following the Middle Eocene Climatic Optimum (MECO) in the central - western Tethys, Paleoceanography, 25, PA3210, doi:10.1029/2009PA001738, 2010.
Stefani, C. and Grandesso, P.: Studio preliminare di due sezioni del Flysch bellunese, Rend. Soc. Geol. It., 14, 157-162, 1991.
Stillman, J. H., and Paganini, A. W., Biogeochemical adaptation to ocean acidifcation, J. Exper. Biology, 218, 1946-1955, doi:10.1242/jeb.115584, 2015.
Stoll, H.M., and Bains, S.: Coccolith Sr/Ca records of productivity during the Paleocene–Eocene thermal maximum from theWeddell Sea. Paleoceanography, 18(2), 1049, doi:10.1029/2002PA000875, 2003.
Tagliabue, A., and L. Bopp: Towards understanding global variability in ocean carbon-13, Global Biogeochem. Cycles, 22, GB1035, doi:10.1029/2007GB003037, 2008.
Thierstein, H. R., Geitzenauer, K. R., Molfino, B., and Shackleton, N. J.: Global synchroneity of late Quaternary coccolith datum levels: validation by oxygen isotopes, Geology, 5, 400-404, 1977.
Thibault, N. and Gardin, S.: The calcareous nannofossil response to the end-Cretaceous warm event in the tropical Pacific, Palaeogeogr. Palaeoclimatol. Palaeoecol., 291, 239-252, doi:10.1016/j.palaeo.2010.02.036, 2010.
Tipple, B. J., Pagani, M., Krishnan, S., Dirghangi, S. S., Galeotti, S., Agnini, C., Giusberti, L., and Rio, D.: Coupled high-resolution marine and terrestrial records of carbon and hydrologic cycles

variations during the Paleocene-Eocene Thermal Maximum (PETM), Earth Planet. Sci. Lett., 311, 82-92, doi:10.1016/j.epsl.2011.08.045, 2011.
Toffanin, F., Agnini, C., Fornaciari, E., Rio, D., Giusberti, L., Luciani, V., Spofforth, D. J. A., and Pälike, H.: Changes in calcareous nannofossil assemblages during the Middle Eocene Climatic Optimum: clues from the central-western Tethys (Alano section, NE Italy), Mar. Micropaleontol., 81, 22-31, doi:10.1016/j.marmicro.2011.07.002, 2011.
Toffanin, F., Agnini, C., Rio, D., Acton, G., and Westerhold, T.: Middle Eocene to early Oligocene calcareous nannofossil biostratigraphy at IODP Site U1333 (equatorial Pacific), Micropaleontol., 59, 69-82, 2013.
Tremolada, F. and Bralower, T. J.: Nannofossil assemblage fluctuations during the Paleocene–Eocene Thermal Maximum at Sites 213 (Indian Ocean) and 401 (North Atlantic Ocean): palaeoceanographic implications, Mar. Micropaleontol., 52, 107-116, doi:10.1016/j.marmicro.2004.04.002, 2004.
Vandenberghe, N., Hilgen, F. J., and Speijer, R. P.: The Paleogene Period, in: The Geologic Time Scale 2012, Amsterdam, the Netherlands (Elsevier BV), 855–922, 2012.
Watkins, D. K. and Self-Trail, J. M.: Calcareous nannofossil evidence for the existence of the Gulf Stream during the late Maastrichtian, Paleoceanography, 20, Pa3006, doi:10.1029/2004pa001121, 1992.
Wei, W., and Wise Jr. S. W.: Biogeographic gradients of middle Eocene–Oligocene calcareous nannoplankton in the South Atlantic Ocean, Palaeogeogr. Palaeoclimatol. Palaeoecol., 79, 29-61, 1990.
Westerhold, T., Röhl, U., Raffi, I., Fornaciari, E., Monechi, S., Reale, V., Bowles, J., and Evans, H. F.: Astronomical calibration of the Paleocene time, Palaeogeogr. Palaeoclimatol. Palaeoecol., 257, 377-403, doi:10.1016/j.palaeo.2007.09.016, 2008.
Westerhold, T., Röhl, U., Donner, B., McCarren, H.K. and Zachos, J.C.: A complete high - resolution Paleocene benthic stable isotope record for the central Pacific (ODP Site 1209). Paleoceanography, 26, PA2216,doi:10.1029/2010PA002092, 2011
Winter, A., Jordan, R.W., and Roth, P.H.: Biogeography of living coccolithophores. in: Coccolithophores edited by Winter, A., and Siesser, W.G., Cambridge Univ. Press, Cambridge , 161-177, 1994.
Winterer, E. L. and Bosellini, A.: Subsidence and sedimentation on Jurassic passive continental margin, Southern Alps, Italy, Am. Assoc. Petr. Geol. Bull., 65, 394-421, 1981.
Young, J. R., Geisen, M., and Probert, I.: A review of selected aspects of coccolithophore biology with implications for paleobiodiversity estimation, Micropaleontology, 51, 267-288, 2005.,
Zachos, J.C., Kroon, D., Blum, P., et al.: Early Cenozoic Extreme Climates: The Walvis Ridge Transect. Proc. Ocean Drill. Program, Initial Rep. 208 doi:10.2973/odp.proc.ir.208.2004, 2004.
Zachos, J. C., Röhl, U., Schellenberg, S. A., Sluijs, A., Hodell, D. A., Kelly, D. C., Thomas, E., Nicolo, M., Raffi, I., Lourens, L. J., McCarren, H., and Kroon, D.: Rapid acidification of the ocean during the Paleocene-Eocene Thermal Maximum, Science 308, 1611-1615, doi:10.1126/science.1109004, 2005.
Zachos, J. C., Dickens, G. R., and Zeebe, R. E.: An early Cenozoic perspective on greenhouse warming and carbon-cycle dynamics, Nature, 451, 279-283, doi:10.1038/nature06588, 2008.
Zachos, J. C., McCarren, H., Murphy, B., Röhl, U., and Westerhold, T.: Tempo and scale of late Paleocene and early Eocene carbon isotope cycles: Implications for the origin of hyperthermals. Earth Planet. Sci. Lett., 299, 242-249, doi:10.1016/j.epsl.2010.09.004, 2010.
Zattin, M., Cuman, A., Fantoni, R., Martin, S., Scotti, P., and Stefani, C.: From middle Jurassic heating to Neogene cooling: The thermochronological evolution of the southern Alps, Tectonophysics, 414, 191-202, doi:10.1016/j.tecto.2005.10.020, 2006.

Zeebe, R. E. and Westbroek, P.: A simple model for the $CaCO_3$ saturation state of the ocean: The "Strangelove", the "Neritan", and the "Cretan" ocean, Geochem. Geophys. Geosyst., 4, 1104, doi:10.1029/2003GC000538, 2003, 2003.

Zeebe, R. E., Zachos, J. C., and Dickens, G. R.: Carbon dioxide forcing alone insufficient to explain Paleocene-Eocene Thermal Maximum warming, Nature Geosci., 2, 576-580, doi:10.1038/NGEO578, 2009.

Ziveri, P., Young, J., and van Hinte J. E.: Coccolithophore export production and accumulation rates. in: On determination of sediment accumulation rates, GeoResearch Forum, Trans Tech Publications LTD, Switzerland, 5, 41-56, 1999.

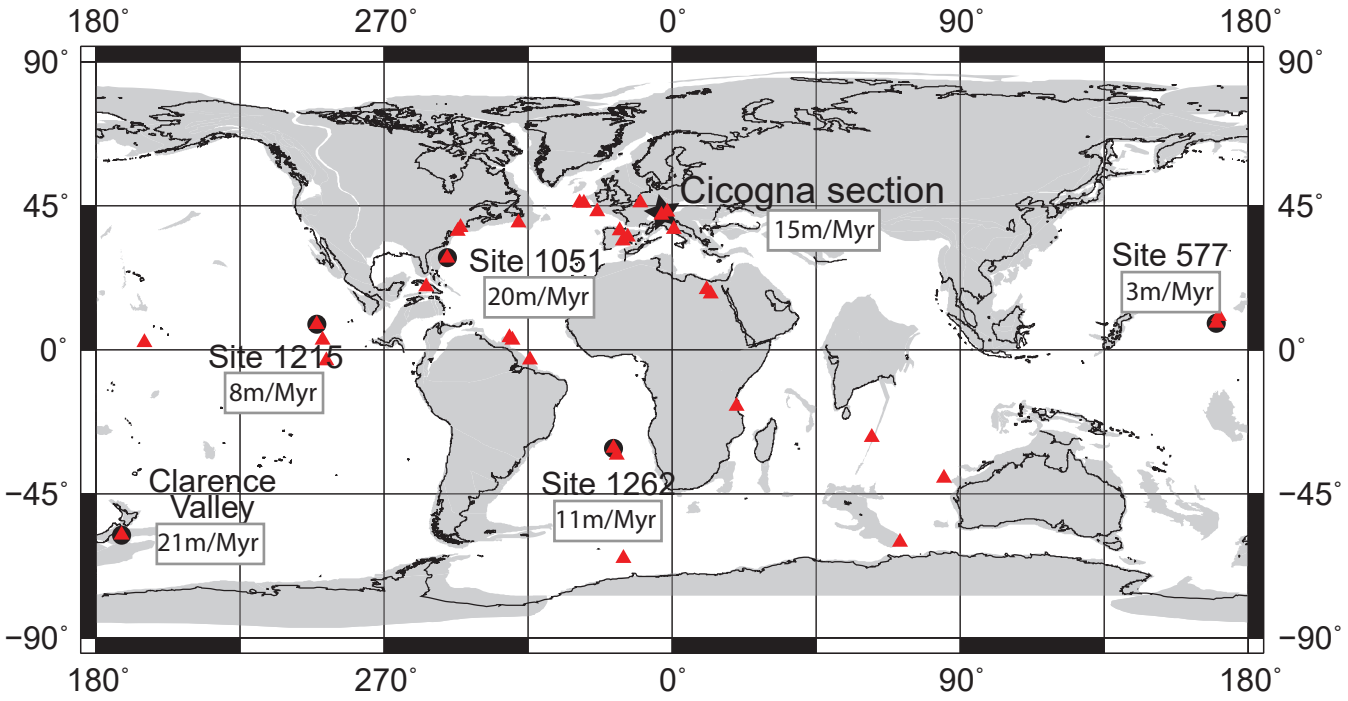


Figure 2_Agnini et al.

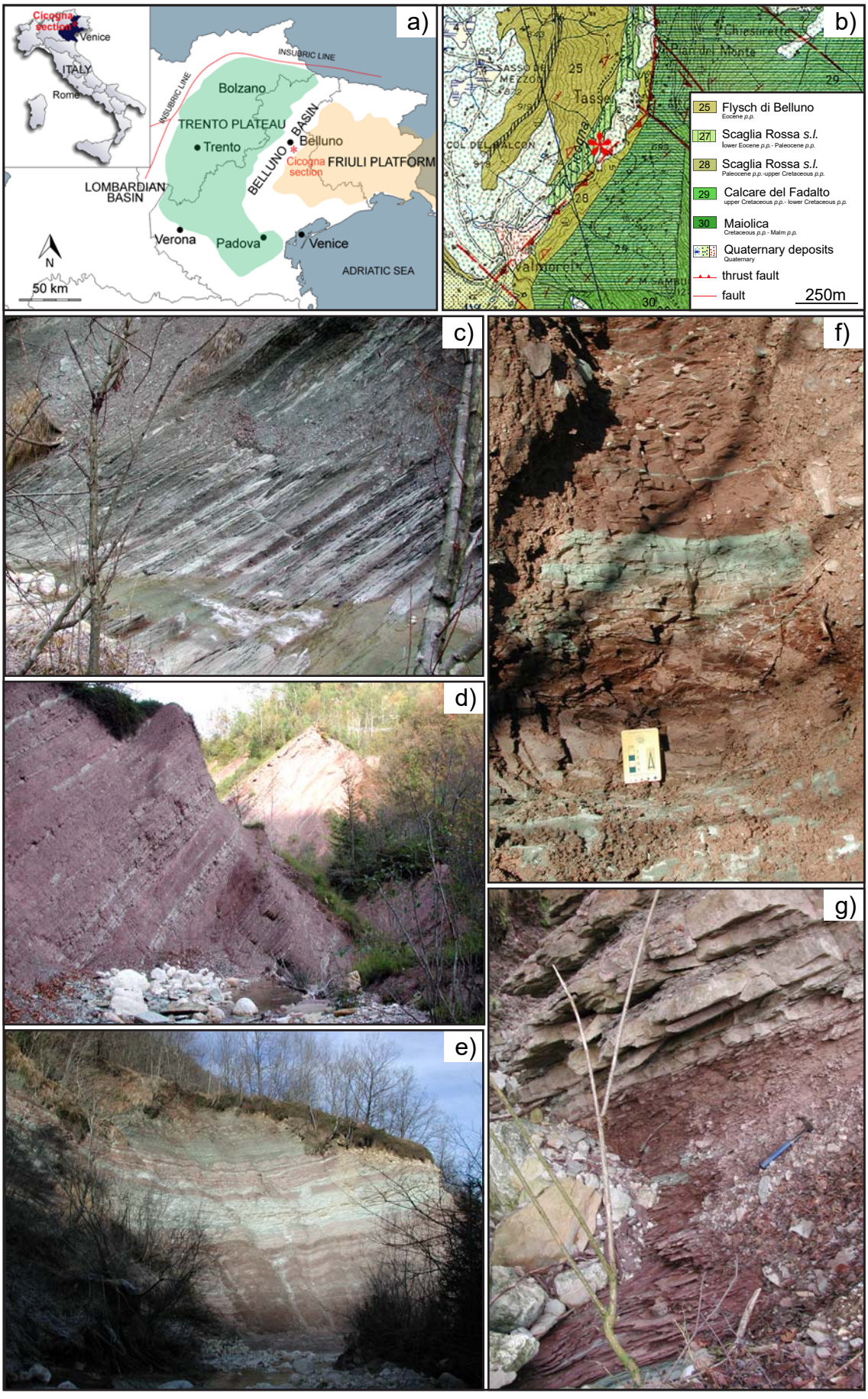


Figure 3_Agnini et al.

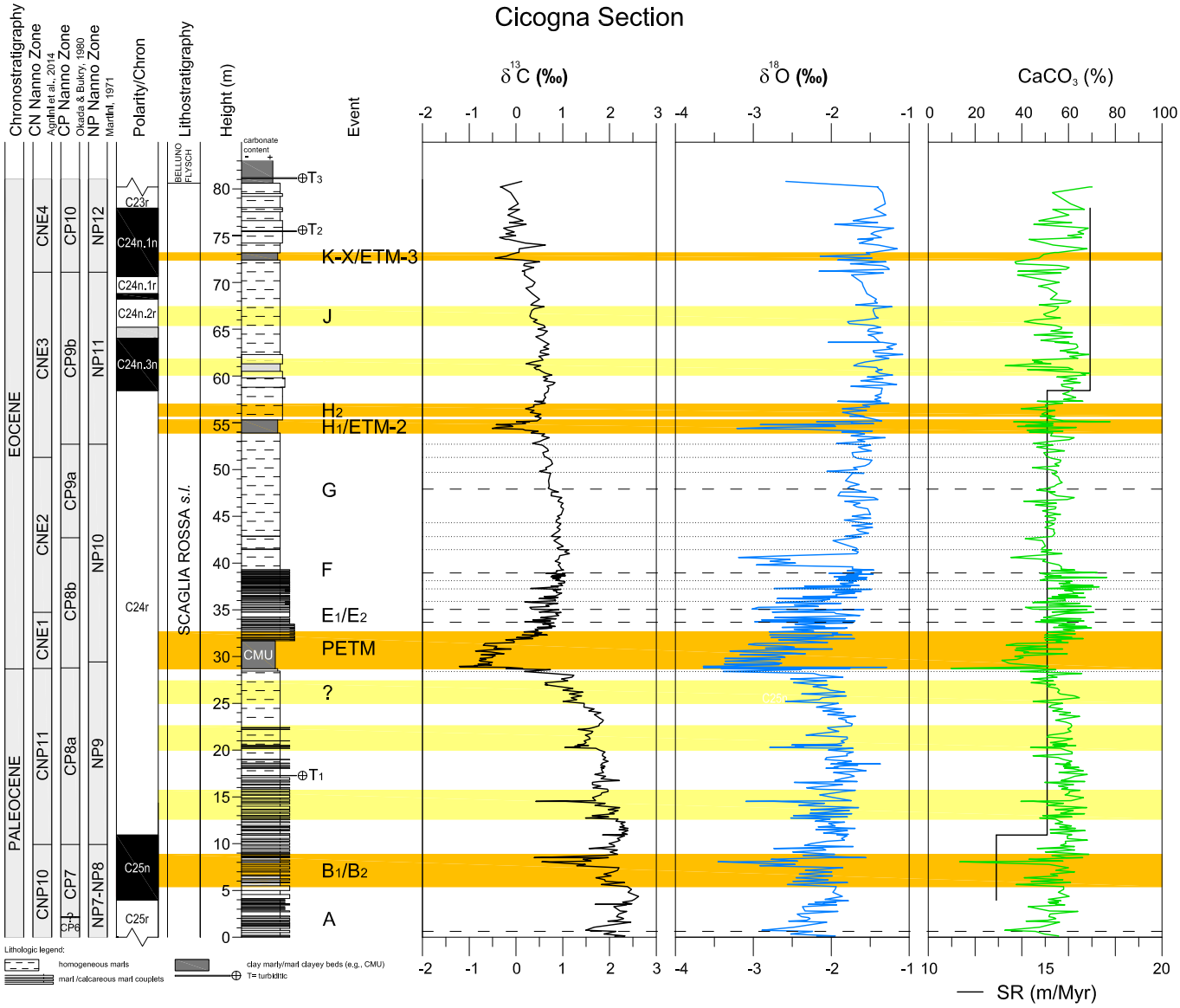


Figure 4_Agnini et al

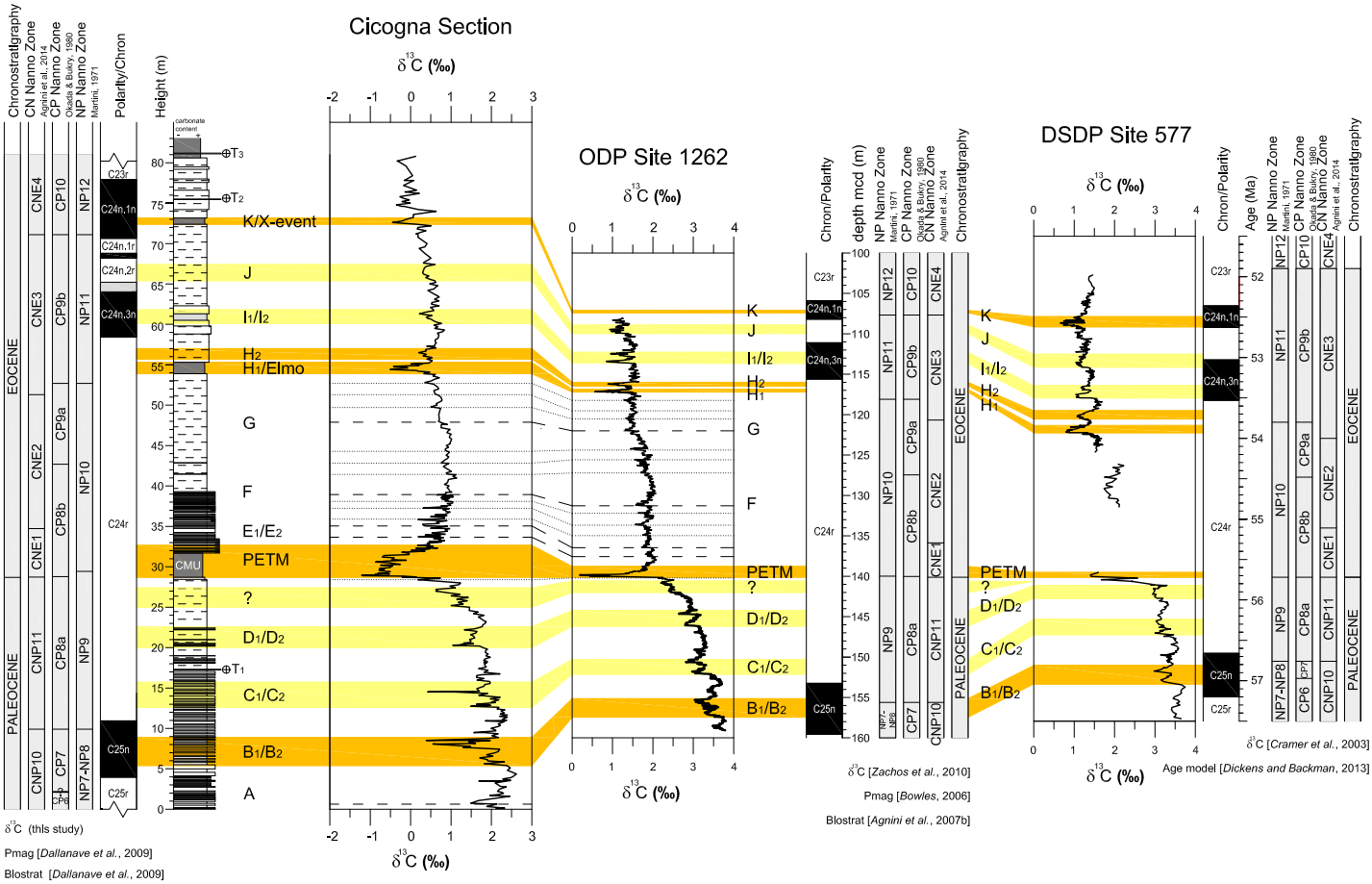


Figure 5_ Agnini et al.

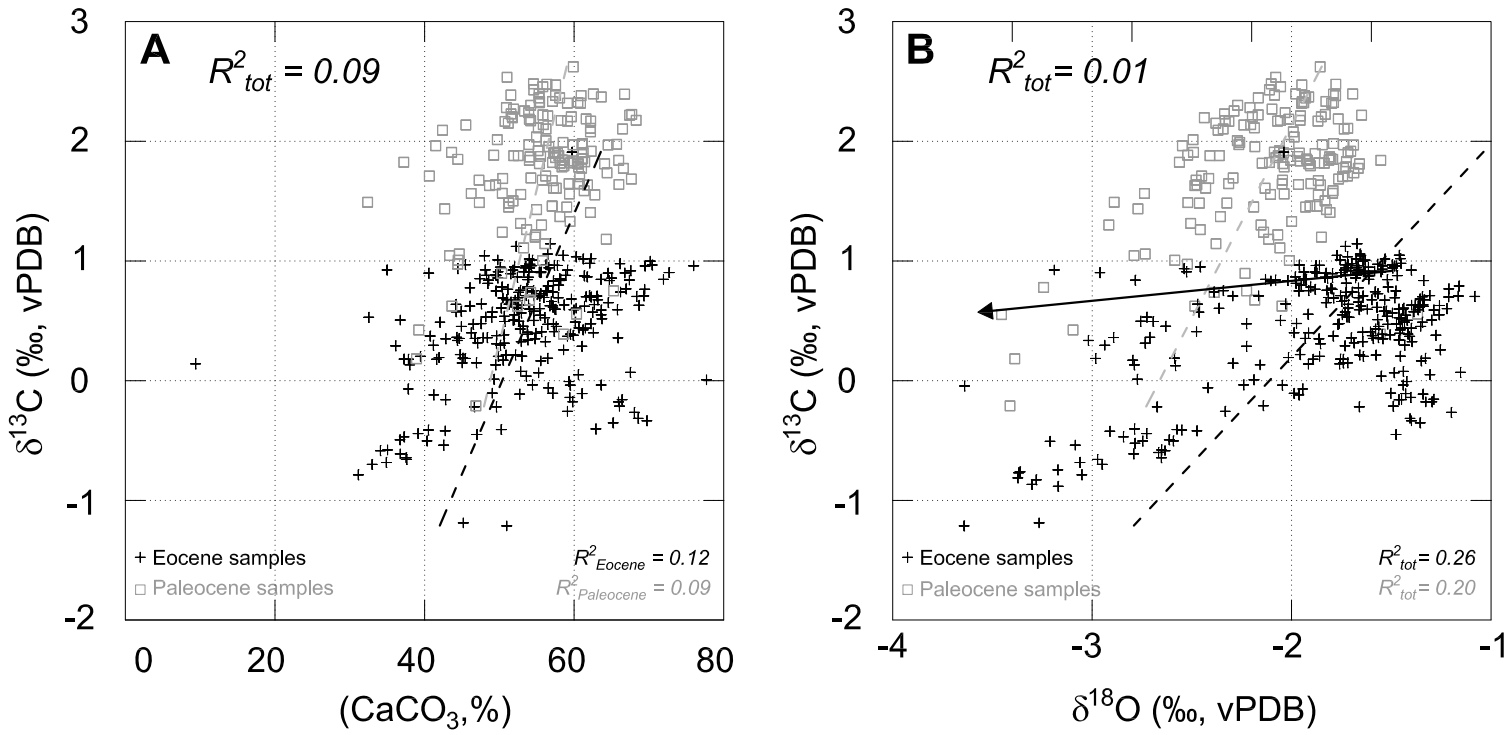


Figure 6_Agnini et al.

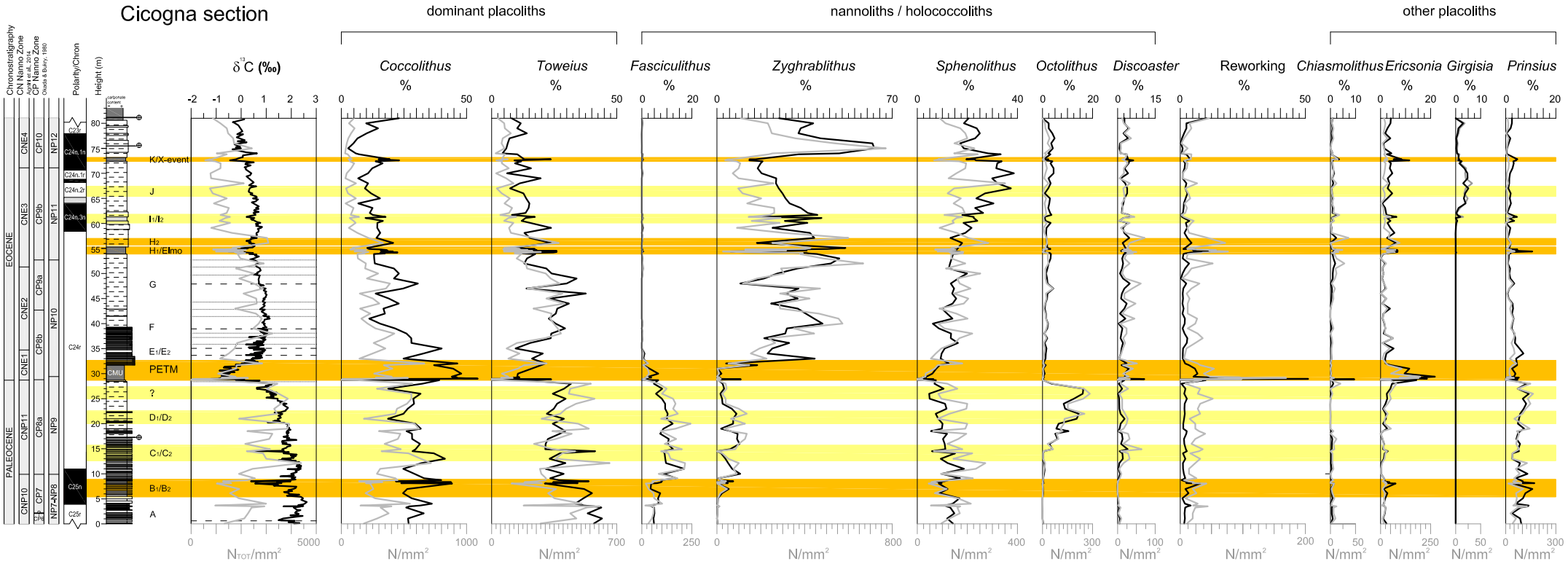


Figure 7_Agnini et al.

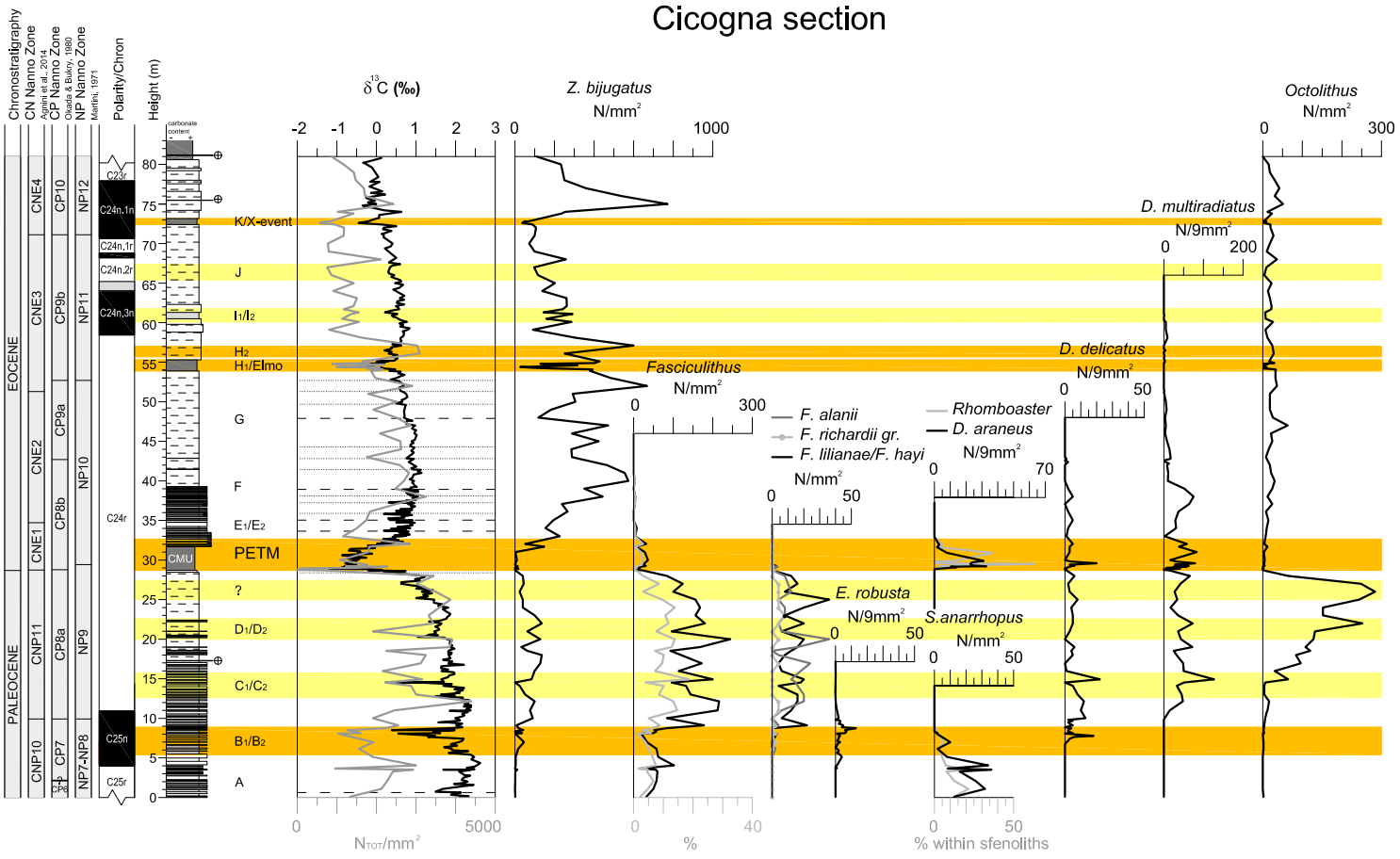


Figure 8_Agnini et al.

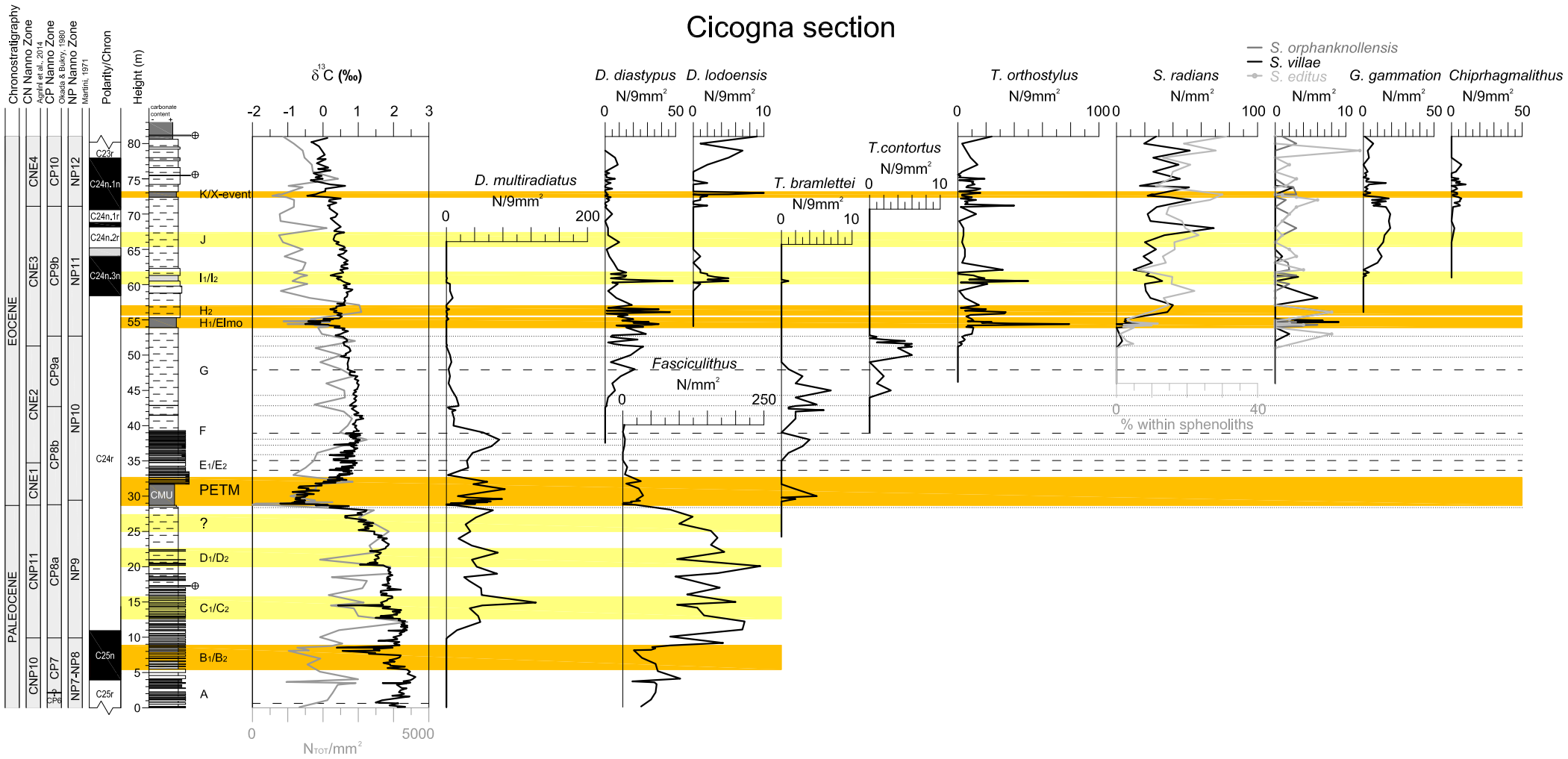


Figure9_Agnini et al.

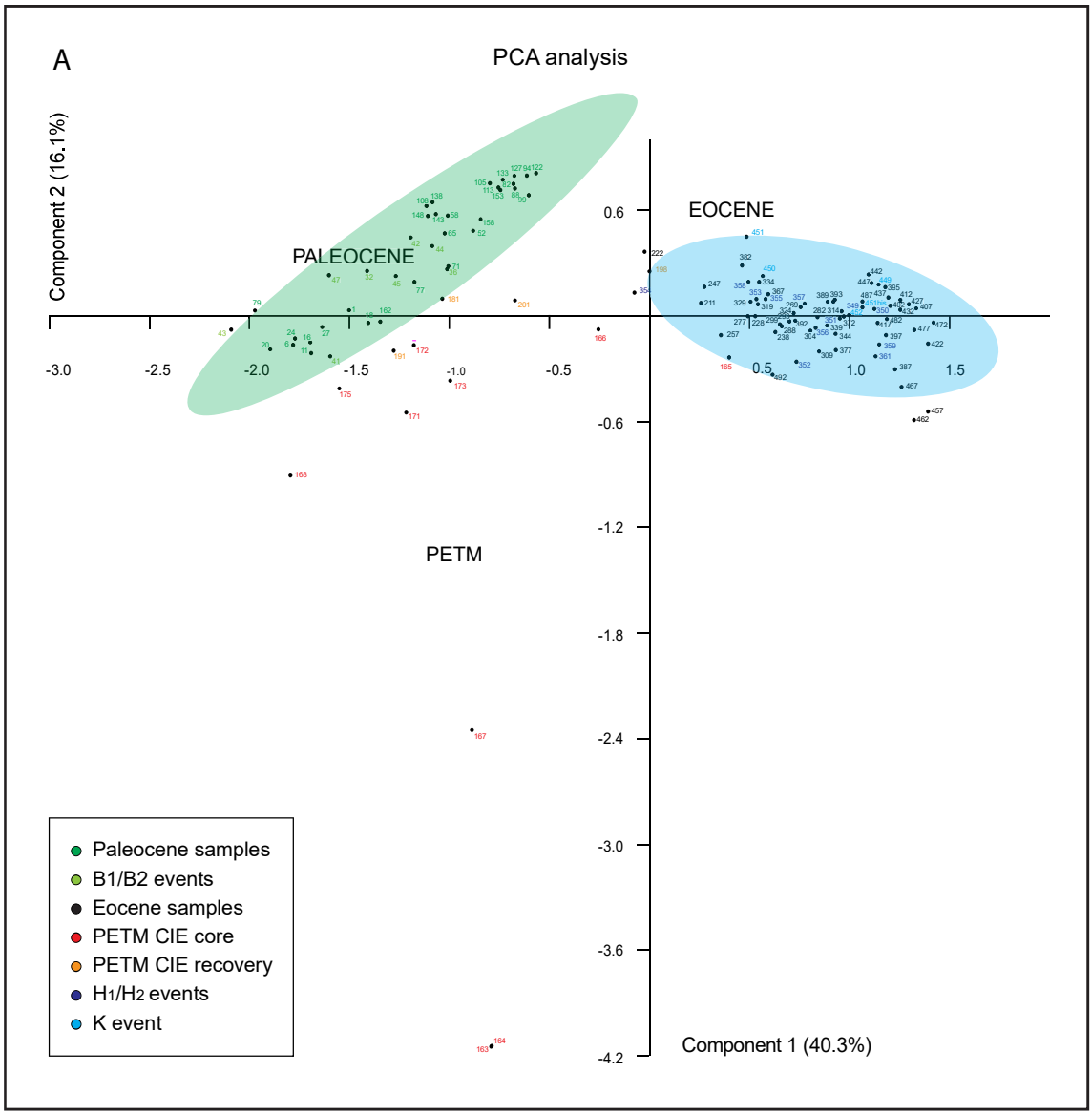


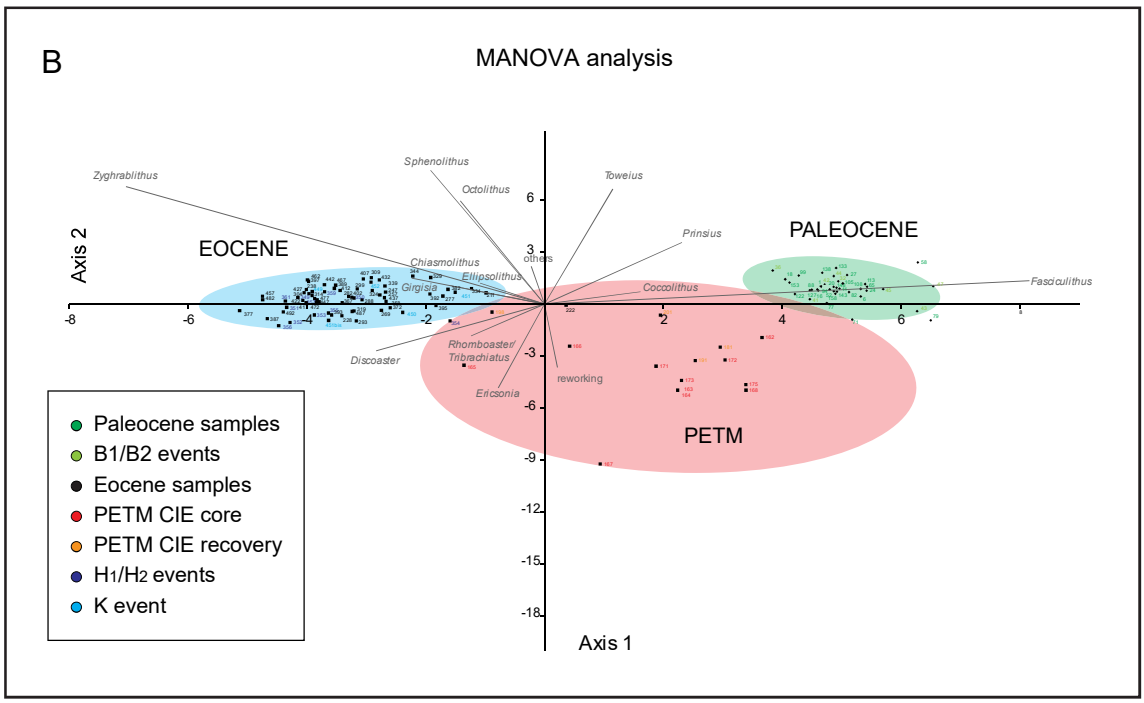


Figure 10_Agnini et al.

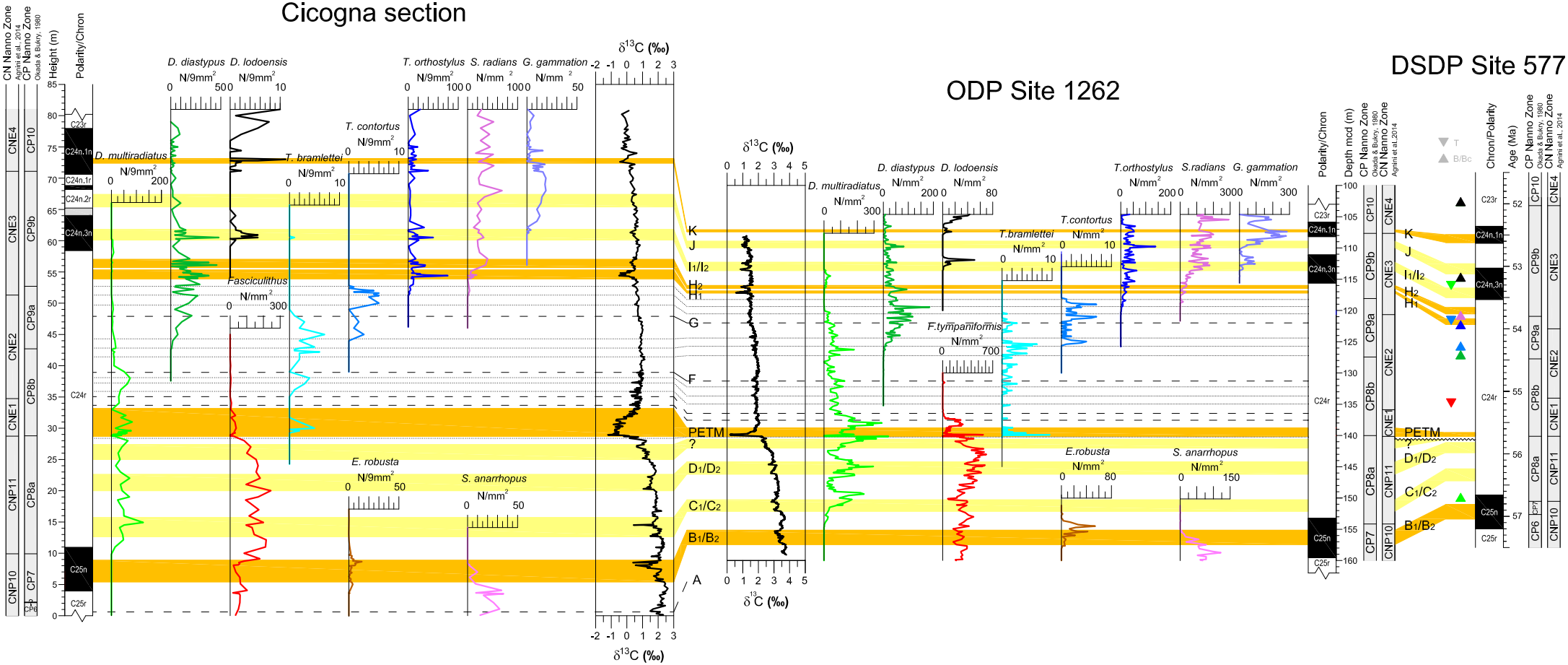


Figure 11_ Agnini et al.

**Table 1**

| Event | | Nanno Zones | | | Cicogna section | | DAMR09I | | W01 | CK95 | GTS04 | GTS12 | Site 1262 | | AG07+/This study | | W01 | CK95 | GTS04 | GTS12 |
|---|---|---|---|---|---|---|---|---|---|---|---|---|---|---|---|---|---|---|---|---|
| | | NP* | CP^ | CN° | Height (m) | Err (m) | Chron notation | | Age (Ma) | Age (Ma) | Age (Ma) | Age (Ma) | Depth (mcd) | Err (m) | Chron notation | | Age (Ma) | Age (Ma) | Age (Ma) | Age (Ma) |
| | C23r base | | | | 77.94 | | | | 0.000 | 52.364 | 52.364 | 52.648 | 52.620 | 105.88 | | | 0.000 | 52.364 | 52.364 | 52.648 | 52.620 |
| | K-X base | | | | 72.20 | 0.10 | C24n.1n | | 0.786 | 52.57 | 52.60 | 52.93 | 52.98 | - | - | - | - | - | - | - | - |
| B | *Discoaster lodoen* | NP12 | CP10 | | 71.10 | 0.10 | C24n.1n | | 0.936 | 52.61 | 52.64 | 52.98 | 53.05 | 107.67 | 0.18 | C24n.1n | 0.777 | 52.57 | 52.60 | 52.92 | 52.97 |
| Bc | *Chiprhagmalithus spp.* | | | | 71.10 | 0.10 | C24n.1n | | 0.936 | 52.61 | 52.64 | 52.98 | 53.05 | 107.67 | 0.18 | C24n.1n | 0.777 | 52.57 | 52.60 | 52.92 | 52.97 |
| | C24n.1n base | | | | 70.64 | | | | 0.000 | 52.630 | 52.663 | 53.004 | 53.074 | 108.19 | | | 0.000 | 52.630 | 52.663 | 53.004 | 53.074 |
| | C24n.1r base | | | | 68.80 | | | | 0.000 | - | 52.757 | 53.116 | 53.199 | - | | | 0.000 | - | 52.757 | 53.116 | 53.199 |
| | C24n.2n base | | | | 68.21 | | | | 0.000 | - | 52.801 | 53.167 | 53.274 | - | | | 0.000 | - | 52.801 | 53.167 | 53.274 |
| B | *Chiprhagmalithus spp.* | | | | 66.50 | 0.50 | C24n.2r | | 0.473 | 52.82 | 52.85 | 53.22 | 53.34 | 109.22 | 0.10 | C24n.2r/.1r | 0.358 | 52.77 | 52.75 | 53.11 | 53.20 |
| | J base | | | | 65.40 | 0.10 | C24n.2r | | 0.778 | 52.94 | 52.88 | 53.26 | 53.38 | 109.96 | 0.02 | C24n.2r/.1r | 0.616 | 52.88 | 52.81 | 53.18 | 53.28 |
| | C24n.2r base | | | | 64.60 | | | | 0.000 | 53.030 | 52.903 | 53.286 | 53.416 | 111.06 | | | 0.000 | 53.03 | 52.903 | 53.286 | 53.416 |
| B | *Girgisia gammation* | | | | 61.20 | 0.10 | C24n.3n | | 0.526 | 53.29 | 53.14 | 53.56 | 53.71 | 113.52 | 0.11 | C24n.3n | 0.540 | 53.30 | 53.14 | 53.57 | 53.72 |
| Br | *Discoaster lodoensis* | | | | 60.40 | 0.10 | C24n.3n | | 0.650 | 53.36 | 53.19 | 53.63 | 53.78 | 113.52 | 0.11 | C24n.3n | 0.540 | 53.30 | 53.14 | 53.57 | 53.72 |
| T | *Discoaster multiradiatus* | | | | 60.20 | 0.10 | C24n.3n | | 0.681 | 53.37 | 53.21 | 53.64 | 53.80 | 113.52 | 0.11 | C24n.3n | 0.540 | 53.30 | 53.14 | 53.57 | 53.72 |
| | I1/I2 base | | | | 60.10 | 0.10 | C24n.3n | | 0.697 | 53.38 | 53.21 | 53.65 | 53.81 | 113.66 | 0.02 | C24n.3n | 0.570 | 53.32 | 53.16 | 53.58 | 53.74 |
| | C24n.3n base | | | | 58.14 | | | | 0.000 | 55.530 | 53.347 | 53.808 | 53.983 | 115.61 | | | 0.000 | 53.530 | 53.347 | 53.808 | 53.983 |
| | H1-Elmo/H2 base | | | | 53.90 | 0.10 | C24r | | 0.090 | 53.81 | 53.58 | 54.06 | 54.26 | 117.21 | 0.01 | C24r | 0.042 | 53.66 | 53.46 | 53.93 | 57.12 |
| T | *Tribrachiatus cont* | NP11 | CP9b | | 52.70 | 0.10 | C24r | | 0.115 | 53.89 | 53.64 | 54.14 | 54.34 | 118.09 | 0.10 | C24r | 0.066 | 53.74 | 53.52 | 54.00 | 57.14 |
| Tc | *Discoaster multiradiatus* | | | | 51.50 | 0.10 | C24r | | 0.141 | 53.97 | 53.71 | 54.21 | 54.42 | 119.38 | 0.11 | C24r | 0.100 | 53.84 | 53.60 | 54.09 | 57.16 |
| B | *Sphenolithus radians* | | | | 51.30 | 0.10 | C24r | | 0.145 | 53.98 | 53.72 | 54.22 | 54.43 | 118.72 | 0.10 | C24r | 0.083 | 53.79 | 53.56 | 54.04 | 57.15 |
| B | *Tribrachiatus orthostylus* | | | CNE3 | 51.30 | 0.10 | C24r | | 0.145 | 53.98 | 53.72 | 54.22 | 54.43 | 120.67 | 0.10 | C24r | 0.134 | 53.95 | 53.69 | 54.19 | 57.18 |
| T | *Tribrachiatus bramlettei* | | | | 48.50 | 0.50 | C24r | | 0.204 | 54.17 | 53.87 | 54.39 | 54.62 | 121.30 | 0.11 | C24r | 0.151 | 54.00 | 53.73 | 54.24 | 57.18 |
| B | *Tribrachiatus contortus* | | CP9a | | 45.50 | 0.50 | C24r | | 0.268 | 54.37 | 54.03 | 54.57 | 54.82 | 125.50 | 0.10 | C24r | 0.263 | 54.35 | 54.02 | 54.56 | 57.25 |
| B | *Discoaster diastypus* | | CP9a | | 42.70 | 0.10 | C24r | | 0.327 | 54.55 | 54.18 | 54.74 | 55.00 | 127.45 | 0.10 | C24r | 0.314 | 54.51 | 54.15 | 54.71 | 57.28 |
| B | *Tribrachiatus bran* | NP10 | | | 35.58 | 0.55 | C24r | | 0.478 | 55.03 | 54.57 | 55.17 | 55.47 | 133.34 | 0.11 | C24r | 0.471 | 55.00 | 54.55 | 55.15 | 57.36 |
| T | *Fasciculithus spp./F. tympaniformis* | | | CNE2 | 34.73 | 0.13 | C24r | | 0.496 | 55.08 | 54.61 | 55.22 | 55.53 | 135.87 | 0.11 | C24r | 0.538 | 55.21 | 54.72 | 55.35 | 57.40 |
| T | *Rhomboaster spp.* | | | | 32.52 | 0.48 | C24r | | 0.543 | 55.23 | 54.73 | 55.36 | 55.67 | 139.72 | 0.01 | C24r | 0.640 | 55.53 | 54.98 | 55.64 | 57.46 |
| X | *Fasciculithus / Zygrhablithus* | | | | 31.60 | 0.10 | C24r | | 0.562 | 55.29 | 54.78 | 55.41 | 55.74 | 139.80 | 0.02 | C24r | 0.643 | 55.54 | 54.99 | 55.64 | 57.46 |
| Br | *Tribrachiatus bramlettei* | | | | 29.43 | 0.18 | C24r | | 0.608 | 55.43 | 54.90 | 55.55 | 55.88 | 139.99 | 0.02 | C24r | 0.648 | 55.56 | 55.00 | 55.66 | 57.46 |
| B | *Discoaster araneus* | | | | 28.95 | 0.05 | C24r | | 0.618 | 55.47 | 54.93 | 55.57 | 55.91 | - | - | - | - | - | - | - | - |
| B | *Rhomboaster spp.* | NP9b | CP8b | | 28.88 | 0.03 | C24r | | 0.620 | 55.47 | 54.93 | 55.58 | 55.92 | 140.02 | 0.01 | C24r | 0.648 | 55.56 | 55.01 | 55.66 | 57.46 |
| | PETM | | | | 28.73 | 0.03 | C24r | | 0.623 | 55.48 | 54.94 | 55.59 | 55.93 | 140.13 | 0.02 | C24r | 0.652 | 55.57 | 55.01 | 55.67 | 57.46 |
| | P/E boundary (extrapolated) | | | | 28.73 | 0.03 | C24r | | 0.623 | 55.48 | 54.94 | 55.59 | 55.93 | 140.13 | 0.02 | C24r | 0.652 | 55.57 | 55.01 | 55.67 | 57.46 |
| decrease | *Fasciculithus spp.* | | | | 28.73 | 0.03 | C24r | | 0.623 | 55.48 | 54.94 | 55.59 | 55.93 | 140.13 | 0.02 | C24r | 0.652 | 55.57 | 55.01 | 55.67 | 57.46 |
| T | *F. richardii gr.* | | | CNE1 | 28.73 | 0.03 | C24r | | 0.623 | 55.48 | 54.94 | 55.59 | 55.93 | 140.13 | 0.02 | C24r | 0.652 | 55.57 | 55.01 | 55.67 | 57.46 |
| | ? base | | | | 25.00 | 0.10 | C24r | | 0.702 | 55.73 | 55.14 | 55.81 | 56.17 | 142.00 | 0.02 | C24r | 0.701 | 55.72 | 55.14 | 55.81 | 57.49 |
| | D1/D2 base | | | | 20.00 | 0.10 | C24r | | 0.808 | 56.06 | 55.41 | 56.12 | 56.50 | 146.17 | 0.02 | C24r | 0.812 | 56.07 | 55.42 | 56.13 | 57.55 |
| | C1/C2 base | | | | 12.61 | 0.10 | C24r | | 0.964 | 56.55 | 55.81 | 56.56 | 56.99 | 152.08 | 0.02 | C24r | 0.969 | 56.56 | 55.82 | 56.58 | 57.64 |
| T | *Ericsonia robusta* | | | | 11.2 | 0.2 | C24r | | 0.994 | 56.64 | 55.89 | 56.65 | 57.08 | 153.32 | 0.10 | C25n | 0.011 | 56.67 | 55.91 | 56.67 | 57.11 |
| | C24r base | | | | 10.93 | | | | 0.000 | 56.660 | 55.904 | 56.665 | 57.101 | 153.25 | | | 0.000 | 56.660 | 55.904 | 56.665 | 57.101 |
| Bc | *F. alanii* | | | | 10.51 | 0.49 | C25n | | 0.060 | 56.69 | 55.93 | 56.70 | 57.13 | 152.77 | 0.02 | C24r | 0.987 | 56.62 | 55.87 | 56.63 | 57.65 |
| B | *Discoaster multira* | NP9a | | | 9.90 | 0.10 | C25n | | 0.147 | 56.74 | 55.98 | 56.74 | 57.18 | 154.61 | 0.11 | C25n | 0.216 | 56.78 | 56.01 | 56.78 | 57.22 |
| Tc | *Sphenolithus anarrhopus* | | | | 8.62 | 0.49 | C25n | | 0.331 | 56.84 | 56.07 | 56.84 | 57.28 | 155.03 | 0.11 | C25n | 0.283 | 56.81 | 56.04 | 56.81 | 57.26 |
| B | *Discoaster delicatus gr.* | | | | 6.86 | 0.12 | C25n | | 0.583 | 56.97 | 56.19 | 56.97 | 57.42 | 156.92 | 0.11 | C25n | 0.583 | 56.97 | 56.19 | 56.97 | 57.42 |
| | B1/B2 base | | | | 5.41 | 0.10 | C25n | | 0.791 | 57.08 | 56.29 | 57.07 | 57.54 | 158.37 | 0.02 | C25n | 0.813 | 57.10 | 56.30 | 57.08 | 56.52 |
| B | *Ericsonia robusta* | | | | 3.97 | 0.07 | C25n | | 0.998 | 57.20 | 56.39 | 57.18 | 57.65 | 158.00 | 0.11 | C25n | 0.754 | 57.06 | 56.27 | 57.05 | 57.52 |
| | C25n base | | | | 3.96 | | | | 0.000 | 57.197 | 56.391 | 57.180 | 57.656 | 159.55 | | | 0.000 | 57.197 | 56.391 | 57.180 | 57.656 |
| B | *Discoaster nobilis gr.* | | CP7 | | 2.14 | 0.05 | C25r | | | 57.337 | 56.518 | 57.314 | 57.801 | 157.35 | 0.10 | C25n | 0.651 | 57.01 | 56.22 | 57.00 | 57.46 |
| B | *D. mohleri* | NP7 | CP6 | | - | - | - | | - | - | - | - | - | 171.50 | 0.11 | C25r | 0.984 | 58.53 | 58.53 | 58.53 | 58.53 |
| | C25r base | | | | - | | | | 0.000 | 58.550 | 57.554 | 58.379 | 58.959 | 171.70 | | | 0.000 | 58.550 | 57.554 | 58.379 | 58.959 |

Reference calcareous nannofossill biozonations: *NP (Martini, 1971); ^CP (Okada and Bukry, 1980); ° CN (Agnini et al., 2014)

Reference timescales: W01 (Westerhold et al., 2008- option1); CK95 (Cande and Kent, 1995); GTS04 (Ogg and Smith, 2004); GTS12 (Ogg, 2012)

IDARM09 (Dallanave et al., 2009)

+AG07 (Agnini et al., 2007)